Universidad del País Vasco Euskal Herriko Unibertsitatea
BILBOKO INGENIARITZA ESKOLA
ESCUELA DE INGENIERÍA DE BILBAO

**MÁSTER UNIVERSITARIO EN**

**CIENCIA Y TECNOLOGÍA ESPACIAL**

# TRABAJO FIN DE MÁSTER

# DINÁMICA DE LA ATMÓSFERA DE MARTE CON IMÁGENES DE VMC/MARS EXPRESS

**Estudiante:** ***García Morales, Josu***
**Director:** ***Sánchez Lavega, Agustín***
**Departamento de Física Aplicada**
**Curso académico** ***2019/2020***

***Bilbao, 14 de septiembre de 2020***

# INDEX

# 1. ABSTRACT

The Mars Express mission of the European Space Agency (ESA) has been in the orbit of Mars since 2003 and has made great contributions to improve the existent knowledge about the red planet. Two of the instruments of this spacecraft are the Visual Monitoring Camera (VMC) and the High Resolution Stereo Camera (HRSC). The main objective of this project has been to study the different dynamical features (hazes, clouds, dust arcs, dust storms) that can be seen in the north polar region of the planet during the spring season (Ls= $0^o$-$90^o$) of the northern hemisphere in the 35th MY (Martian Year). In addition to taking measurements of these structures, a theoretical analysis of the obtained results has been done using tools like the Mars Climate Database (MCD).

La misión Mars Express de la Agencia Espacial Europea (ESA) lleva en la órbita de Marte desde el año 2003 y ha contribuido a aumentar el conocimiento existente sobre el planeta rojo. Dos de los instrumentos de esta nave son la Visual Monitoring Camera (VMC) y la High Resolution Stereo Camera (HRSC). El objetivo de este trabajo ha sido el de usar imágenes de esos instrumentos para estudiar las distintas estructuras (neblinas, nubes, arcos de polvo y tormentas de polvo) que se forman en la región polar norte del planeta durante la primavera (Ls= $0^o$-$90^o$) de dicho hemisferio en el año marciano 35. Además de medir estas estructuras se ha realizado un análisis teórico de los resultados obtenidos empleando herramientas como el Mars Climate Database (MCD).

Europako Espazio Agentziaren (ESA) Mars Express misioa 2003tik dago Marteren orbitan eta planeta gorriari buruz dagoen ezagutza handitzera lagundu du. Espazio ontzi honetako bi instrumentu Visual Monitoring Camera (VMC) eta High Resolution Stereo Camera (HRSC) dira. Proiektu honen helburua tresna horien irudiak erabiltzea izan da, marteko 35. urteko hemisferio horren udaberrian (Ls= $0^o$-$90^o$) planetaren iparraldeko eskualde polarrean sortzen diren estrukturak (lainoak, hodeiak, hauts-arkuak eta hauts-ekaitzak) aztertzeko. Egitura horiek neurtzeaz gain, lortutako emaitzen analisi teorikoa egin da, Mars Climate Database (MCD) bezalako tresnak erabiliz.

## 2. KEY WORDS

Mars

Atmosphere

Dust

Dust storm

Water ice

Cloud

Haze

Baroclinic disturbances

# 3. INTRODUCTION

This project is related to some of the subjects of the master but it is not only connected to some subjects, this project is also connected to the scientific research work that it is being done in the Grupo Ciencias Planetarias (GCP) of the UPV/EHU. The connections between this project and the scientific research will be addressed in this part of the document.

A description of the background of the exploration of Mars is also necessary to fully understand the extent of this project, specifically of the Mars Express mission, focusing the interest in some of the instruments that are onboard the spacecraft. Those instruments are the Visual Monitoring Camera (from now on VMC) and the High Resolution Stereo Camera (from now on HRSC). Technical details of those instruments will be presented along with a brief description of the work that has been done with them. Finally, the main objectives of this project will be addressed in extent to end this part of the document.

## 3.1 CONTEXT

As it has been told before, this project has well established connections with some of the subjects of the master. The subject that is most connected to the project is Planetary Atmospheres, in fact this project could be also presented as the study of a small part of the Martian atmosphere, in this case, the part of the atmosphere that it is directly above the north polar region of Mars. During the lectures of that subject the main characteristics of the Martian atmosphere (as well as characteristics of other planetary atmospheres) were addressed. Some concepts that were introduced in that subject have made possible to understand some of the observed atmospheric phenomena. Other concepts have been used to interpret the results that were obtained in the measurements.

Planetary Atmospheres is the main subject in terms of connections with this project, but there have also been other important connections. That is the case of Physics of the Solar System were features of the planets of the solar system were introduced. Regarding Mars, topics like its formation, how the planet was in its early stages or the science that has been done by the different missions developed by the space agencies, were some of the topics discussed. This knowledge has made possible to get a better understanding of how the planet has changed during the years and how that affected to the present Mars.

Another important knowledge gathered in this master was learning how to search and use the vast amount of technical resources that are available in the internet, not only in terms of information, but also in terms of software. For example, in this project a program like GIMP (Image Editor, [5]) has been used to measure distances in the images provided by the HRSC. Other topics that were also addressed in this project are astrodynamics, spacecrafts and their instruments and analysis of the data gathered in a space mission.

## 3.2 EXPLORATION OF MARS

Many space agencies have taken part in the exploration of Mars [w1] during the past decades. Some of these agencies have not been able to accomplish their goal of landing or orbiting Mars but it is always important to invest in this kind of projects in order to encourage the scientific research and the technical developments of the countries involved in those agencies.

The first attempts were made in the early 60s by the Soviet Union. These probes were destined to make a flyby of Mars but all of them failed. It is fair to recognize that one of these spacecrafts, the Mars 1, was the first probe to achieve interplanetary orbit in 1962. This probe did not accomplish its primary mission, but it was able to send data during part of its flight towards Mars. This data allowed to improve the understanding of topics like the terrestrial magnetic field, the solar wind or micrometeorites.

Meanwhile, the United States were also developing their own specific program with the objective of reaching other planets of the solar system. This was the so-called Mariner program, which as has been told, had the mission of sending probes to other planets of the solar system, in this case Mercury, Venus and Mars. Regarding Mars, the Mariner 3 and 4 missions were the first American missions destined to perform a flyby of the red planet. The Mariner 3 was lost during the launch but the Mariner 4 mission achieved its goal in 1965, which allowed it to send the first close-up pictures of Martian surface.

There were other missions of the Mariner program that had Mars as their target, for example, the Mariner 6 and 7 performed two more flybys over the Martian surface. After the successful flybys the next goal was to develop the first orbiter of Mars. This was accomplished by the Mariner 9 mission just two weeks before than the soviet Mars 2 mission, even though the American spacecraft was launched later than the soviet mission.

Once the Mariner program had accomplished its mission the National Aeronautics and Space Administration (NASA) created a new program to carry on with the exploration of the red planet, this was the so-called Viking program. The spacecrafts of this programs consisted in a lander and an orbiter, which served also as communications relay. However, the honour of landing first on the Martian surface it is held by the Mars 3 soviet mission, which landed in 1972 but failed shortly after its touchdown.

During the next decades more missions were sent to the red planet, some of them now not only carried landers but also rovers, which was a key factor in terms of analysing the surface of the planet. The first functional rover on the Martian surface was the Sojourner which was mounted on the Mars Pathfinder's lander. These rovers gave a new perspective and opened a brand-new set of possibilities to the scientists involved in the missions. Now it was possible to explore the planet in three different ways. The orbiters like the Mars Global

Surveyor had cameras that mapped the terrain to study the surface and carried sensors that were able to reveal some of the details of the Martian atmosphere.

The landers studied the atmosphere and the surface at ground-level helping to determine if the planet had the necessary conditions to host some kind of lifeform in the past and the rovers broadened the reach of these landers with their mobility.

With the past of time other countries targeted Mars as a scientific point of interest. In the late 1990s the Japan Aerospace Exploration Agency (JAXA) designed the Nozomi orbiter with the objective of studying the upper Martian Atmosphere and its interaction with the solar wind but it failed and never reached orbit.

In the early 2000s the European Space Agency (ESA) developed its first Martian mission, the Mars Express mission, which will be described with thorough detail further ahead as some of its instruments have been used during this project. In that decade NASA kept its leadership in terms of scientific exploration of the red planet with orbiters like Mars Odyssey and Mars Reconnaissance Orbiter and rovers like Spirit and Opportunity. These rovers made huge scientific contributions and were active for 2208 sols and 5351 sols respectively.

During the 2010s decade two new space agencies tried to reach the red planet, the China National Space Administration (CNSA) sent an orbiter in the Fobos-Grunt mission, which was a combined effort with Roscosmos, but this mission never left LEO. The other agency was the Indian Space Research Organisation, whose Mars Orbiter Mission entered orbit in 2014 and it is still active. In this decade other space agencies continued their efforts, for example, NASA sent the Mars Science Laboratory (also known as Curiosity) towards Mars and it is still active on the surface.

Nowadays, as the 2020 decade begins three more missions have taken advantage of the 2020 launch window to reach Mars. NASA is sending another rover (Perseverance) to the surface and the CNSA (Chinese Space Agency) will try to reach the red planet with an orbiter and a lander. Besides, the United Arab Emirates will make their first attempt to reach Mars with the Emirates Mars Mission. Further ahead, there are plans to bring samples back from the red planet and its moons with hope that this might pave the way to a first manned mission in next decades [w1].

## 3.3 MARS EXPRESS MISSION

Mars Express [1] was not only the first European mission to Mars, but it was also the first European mission to another planet. It was launched from de Baikonur Cosmodrome (Kazakhstan) on top of a Russian Soyuz rocket. This mission took advantage of the 2003 launch window, as well as other missions did, like it was the case of NASA's Mars Exploration Rover missions (Spirit and Opportunity). This launch window gathered some special conditions that made possible this mission, that is to say, another launch window like the 2005 launch window would have made necessary another kind of rocket or a smaller payload.

The mission consisted in an orbiter and a lander named Beagle 2 (Figure 1). The lander was ejected five days before the orbital insertion but its destiny remained unknown because it never sent any transmission to the orbiter or the ground stations at Earth. That changed in 2015 when the Mars Reconnaissance Orbiter (MRO) captured images of the Beagle 2 on the surface. On the other hand, the orbiter had a successful rendezvous with the red planet and it is still operational.

Figure 1. Mars Express with the Beagle 2 still attached [1].

With the failure of the Beagle 2 the mission could not perform all of its scheduled experiments. The instruments onboard the lander were supposed to perform different kind of analyses of the landing area, which was located in the Isidis Planitia (11.6º N, 89.5º E). This is a region considered of a high scientific interest because it is believed that it was flooded by water during its early stages, which might have left behind traces of biological activity.

Putting the lander's failure aside the mission can be considered a huge success taking into account the scientific discoveries that the orbiter has made possible. Some of the objectives of the orbiter were:

- Mapping the surface with better resolution than previous missions.
- Super-resolution of very specific areas.
- Mapping the surface in IR.
- Subsurface structure characterisation.
- Study the global circulation and the atmospheric composition.
- Surface-atmosphere interaction.

During its lifespan Mars Express has completed more than 20000 orbits and it can be said that it has fulfilled its original purposes. Even now it keeps making huge contributions, for example, two years ago the spacecraft detected evidences of subglacial liquid water on Mars [2]. This has settled one of the longest arguments that existed regarding Mars, which was the possible presence of liquid water in its surface.

Nevertheless, Mars Express has also provided insight in other topics that were not originally meant to be explored by this mission, like the study of the Martian moon Phobos using the instruments onboard the ship. For all of this, Mars Express can be considered not only one of the most successful missions of the ESA, but one of the most successful missions in the history of the exploration of the red planet.

Now, the instruments of the spacecraft will be presented but focusing the description in the instruments that have been used in this project, the cameras VMC and HRSC.

### 3.3.1 VMC (Visual Monitoring Camera)

The description of the spacecraft's instruments will begin with a detailed overview of the VMC [3]. VMC is a 640 x 480 pixel colour CMOS type camera with a wide-angle field of view $30^o$ x $40^o$, which makes it very similar to an old PC webcam. The instrument (Figure 2) is composed by an IRIS-1 sensor/camera and the housing where it is mounted. The sensor produces the 640 x 480 pixel images with 8 bits per pixel sampling depth, the images are grayscale by default, but a Bayern pattern filter was equipped to obtain colour information of the images.

Other technical details are the exposure time range and the readout time of the sensor. The exposure time ranges from 0.4 ms to 162.8 ms with 0.8 ms steps and from 200 ms to 95800 ms with 400 ms steps. On the other hand, the readout time of the sensor is 100 ms but there is also a minimum interval between the images due to the time that it takes to transmit the data to the spacecraft's memory.

The housing provides power support and data interface equipment. The whole assembly has a weight of 430 g, with a very low ($\sim 3\ W$) power consumption compared with other instruments ($\sim 30\ W$). VMC is a standard device produced in Belgium by the OIP Sensors Systems company and it has had different designs during the years.

Figure 2. A VMC unit with the protective lens removed and 1 euro for size comparison [3].

The original purpose of the VMC mounted on the spacecraft was to provide confirmation of a correct separation of the Beagle 2 lander. Instead of using sensors to confirm the separation of the lander, the alternative of installing a camera was chosen due to its smaller complexity and better results. At first, it was intended to record the separation event with this camera, but due to some activities connected to the decoupling, the VMC could not been switched on until a few second after the ejection event. This meant that the VMC could only took 4 pictures (Figure 3) of the Beagle 2 lander.

Figure 3. One of the 4 images taken by VMC after the ejection [3].

As it has been told before, some kind of failure occurred during the landing attempt of the Beagle 2. As a result of this failure, an investigation was commissioned to determine what could have failed during the ejection event and the rest of operations performed by the lander. The pictures taken by the VMC after the separation played a major part in this investigation and after a thorough research of them, no anomalies were visible. Therefore, it is still unknown the reason of the lander's failure, there are some possibilities like an unusual thin atmosphere that could have affected the landing or even a damaged heat shield that are valid explanations.

After three years of no activity at all it was proposed that VMC could be used in a different role. Taking into account its field of view, ESA thought that VMC could serve as some kind of "Mars webcam", serving in that way as an interest for the public and the scientific community. However, the operation of VMC has some constraints because it must not interfere with the activities of the spacecraft's instruments. Here are some of the constraints:

- Even its power consumption is really low, it must be taken into account during the observations' planning.
- The images (302 kb per image) must be taken into account at the time of monitoring the solid mass memory of the ship.
- VMC requires a special pointing that interferes with the activities of the rest of instruments, therefore, VMC's observation windows are limited.
- VMC and other instruments cannot be used at the same. This is motivated by the data interface of the VMC, which will send its data regardless of any other data waiting its transmission. This ends up blocking the transmission of other instruments' data.
- The observation windows are usually when the spacecraft is close to the apocentre when thrusters are fired. The thruster's exhaust affects the activity of the instruments but it has no effect on VMC.

With all of these things on the table, VMC was used for the first time as a scientific instrument in 2016 at the initiative of Prof. Sánchez-Lavega (since then, IP of this instrument) and the GCP [12]. It has complemented the work of the other instruments and there are several scientific publications that have used this camera [8, 12, 23]. Not only it has had an outreach in the scientific community but its public outreach has been remarkable with initiatives like a Twitter account [w2] or a Flickr gallery [w3] where anyone has access to the processed images and can enjoy of a spectacular view of the red planet.

### 3.3.2 HRSC (High Resolution Stereo Camera)

Previous missions carried cameras to map the Martian surface, the firsts cameras to do that were onboard NASA's Viking spacecrafts. The Viking's cameras provided an almost global coverage at approximately 200 m/pixel resolution and were able to map smaller areas of the surface with a better coverage. That was also the case of following missions like Mars Observer or the Mars Reconnaissance Orbiter (MRO), for example, MRO's HiRISE instrument can produce images of very small areas with a resolution of 0.3 m/pixel.

The existent gap (in terms of resolution) between the global coverage and the coverage of smaller areas was supposed to be covered by Mars Climate Orbiter's (MCO) camera but this mission failed when it was entering into orbit. MCO was supposed to provide an almost global coverage with 40 m/pixel resolution so its loss created the gap mentioned before. Hence, the responsibility of covering this gap in Mars' imagery fell upon HRSC (Figure 4).

Figure 4. HRSC instrument [5].

HRSC [4 & 5] is designed to map the morphology, topography, structure and geological context of the surface as well as atmospheric phenomena, in fact, this last HRSC's capability has been used in this project. HRSC has also contributed to scan possible landing sites for other missions and has even taken one of the best images to date of Mars' moons.

The HRSC instrument is a multi-sensor pushbroom camera comprising 9 CCD line sensors mounted in parallel for a simultaneous high-resolution stereo, multicolour and multiphase imaging by delivering 9 superimposed image swaths. HRSC can produce images with a resolution up to 10 m/pixel, it has five panchromatic channels and four colour channels and some more details of those channel are listed below and its working principle can be seen in Figure 5:

- 2 stereo channels (S1, S2).
- 2 photometry channels (P1, P2).
- 1 nadir channel (ND).
- BL (blue channel 440 ± 45 nm).
- GR (green channel 530 ± 45 nm).
- RE (red channel 750 ± 20 nm).
- IR (near infrared channel 970 ± 45 nm).

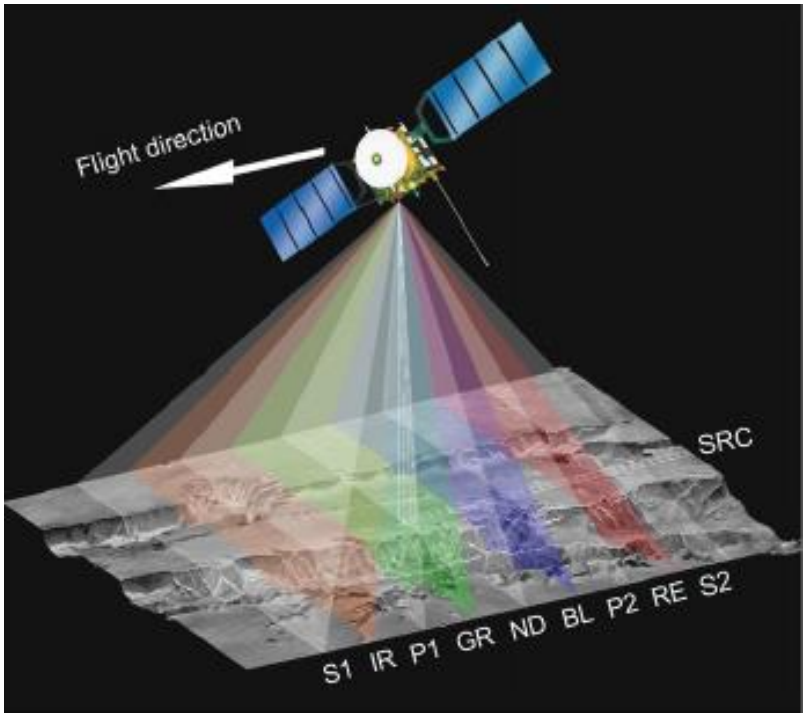


Figure 5. Operating principle and sensors' viewing [4].

As it can be seen in Figure 5 there is another channel, the Super Resolution Channel (SRC), which comprises a 1024 x 1024 CCD array and lightweight mirror optics (Makutsov-Cassegrain telescope). The optics of this channel are allocated under the baffle of the HRSC as it can be seen in Figure 4. This additional channel can produce images with a resolution 5 times higher but it has a really narrow field of view (approximately $0.5^{o}$) so the areas that it can cover are quite small compared with the areas that the HRSC can cover in one swath (up to $10^5$ $km^2$).

A compilation of the work that HRSC has made is done in [5], showing that HRSC has provided the global coverage mentioned before with the necessary resolution. Table 1 shows the percentage of the surface covered by a certain resolution.

| ***Table 1*** | |
|---|---|
| ***Mars mapping coverage*** | |
| **Resolution** | **Percentage** |
| ≤ 100 m/pixel | 97% |
| ≤ 60 m/pixel | 96.5% |
| ≤ 50 m/pixel | 96% |
| ≤ 40 m/pixel | 94.8% |
| ≤ 30 m/pixel | 87.7% |
| ≤ 20 m/pixel | 68.8% |

### 3.3.3 Other instruments

The main objectives of the Mars Express mission have been discussed before so now it is the turn of the instruments that have made that possible. Not all of them are of scientific nature, for example, the spacecraft has a High Gain Antenna to transmit the data back to Earth but now only a short description of the scientific instruments will be given [1]:

- Visible and Infrared Mineralogical Mapping Spectrometer (OMEGA). This instrument is a visible and near-IR mapping spectrometer that is able to characterise the composition of surface materials with a resolution up to a few hundred meters.
- Ultraviolet and Infrared Atmospheric Spectrometer (SPICAM). It is a UV and IR spectrometer with the objective of studying the atmosphere, focusing its work on atmospheric photochemistry, atmospheric escape processes of the upper atmosphere-ionosphere and the interaction of the Martian atmosphere with the solar wind.
- Planetary Fourier Spectrometer (PFS). A double-pendulum spectrometer, whose main scientific objectives are the monitoring of the temperature field in the lower atmosphere, analysis of the chemical composition and optical properties of the atmosphere's aerosols and determination of the thermal inertia.
- Analyzer of Space Plasmas and Energetic Atoms (ASPERA). Focused on the interaction of the upper atmosphere with the interplanetary medium and the solar wind.
- Sub-Surface Sounding Radar Altimeter (MARSIS). A radar sounder and altimeter with ground penetration capabilities. Its main objective is to map the distribution of water (liquid and solid) down to 3-5 km under the surface.
- Mars Radio Science Experiment (MaRS). Performs radio sounding experiments of the Martian atmosphere in order to derive vertical density, pressure and temperature profiles as a function of height. It has also contributed to determine the precise mass of Phobos and to study the solar corona during solar conjunctions.

## 3.4 OBJECTIVES OF THIS PROJECT

The main objective of this project is to study the different kind of meteorological formations that can be seen over the north polar region during the spring season (Ls $0^{o}$ - $90^{o}$) of that hemisphere in the 35th MY. In terms of Earth date, this means that all the structures that have been studied developed in 2019 between the months of March and October. Due to the eccentricity of its orbit the duration of the seasons in Mars it is not the same for both hemispheres. This creates longer springs and summers for the northern hemisphere but they are colder than the austral spring and summer because Mars' aphelion takes place in Ls=$71^{o}$. This has obviously an effect in the insolation received by the surface, therefore, the atmospheric conditions are different for the same season in both hemispheres [w4].

Different kind of formations have been studied and that includes those characterized by dust and those characterized by water ice. Regarding the dust structures, these can be classified between Textured Dust Storms (from now on TDS), Arc Dust Storms (from now on ADS) and spirals (S) due to their shape. Other structures haven been also noted (thin dust patches, small dust clouds) and measured, but they are not the main interest of this project. The other type of structures, the ones characterized by water ice, can be classified in either clouds or hazes with only one exception, the large spiral system seen in the HRSC's images.

With the TDS, the study conducted has consisted in measuring their location (latitude and longitude), the surface they cover and whenever possible their speed has been tried to be determined. Another interesting feature of the TDS is their cells top morphology [6 & 7], which has been studied measuring the size of the cell-like structures that can be seen in the images and also the distance between the different cells in an attempt to search for a pattern distribution. With respect of the spirals their location, main dimensions and speed has been measured. Regarding the ADS, their location and dimensions have been measured and in some remarkable events an attempt of measuring their speed has been done. The approach with the water ice structures has been practically the same measuring their locations and their dimensions.

Once the features have been identified and measured a theoretical analysis of the results has to be done. This means to compare the measurements obtained, with the conditions of the Martian atmosphere predicted by the existent theoretical models and also trying to identify the locations that present more possibilities of developing the kind of phenomena that have been identified. Besides, these theoretical models can be used to make an educated guess of these phenomena's altitude because it was not possible to determine it from the images.

The results of this project will be presented in two scientific conferences and a publication on the subject will be prepared in the future. This is another proof of the connections that this project has with the work that is being done in the UPV/EHU in terms of planetary science.

# 4. METHODOLOGY

In this section, the methodology employed in this project will be addressed. Two types of images have been analysed, the ones taken by VMC and the ones taken by HRSC and two different methods have been used to analyse them. To navigate the VMC's images and to measure them, the Elkano application [8] has been used. In order to measure the HRSC's images the program GIMP [w5] has been used following two different methods.

The other part that will be explained in this section is the methodology followed during the development of the theoretical analysis. To perform this analysis two tools like JMARS [9] and the Mars Climate Database (from now on MCD) [10 & 11] of the Laboratoire de Météorologie Dynamique (LMD) have been used.

## 4.1 ELKANO APPLICATION

The Elkano application allows to navigate the images taken by VMC and allows to perform measurements of the images. But first, in order to select which images have to be analysed, there is also a gallery available [8] which contains images taken by VMC since 2012. There is also an online public gallery (created by ESA) in Flickr [w3] where the raw images of VMC are available. This gallery was used to make a first selection of the images that were of interest for this project but no more work was done with it.

As it has been mentioned the gallery that has been used contains images taken by VMC, but not all of them, only the images that have been taken since 2012. To make an accurate description of this gallery Figure 6 will be of assistance. This figure is a screenshot of the gallery where a few modifications have been made in order to help with the explanation.

In the bottom part of the image it is placed the menu that allows to navigate between the different series of images taken by VMC. Once the series is chosen, to navigate between the series' images, one only needs to use the up/down arrows of the keyboard.

The blue rectangle marked as 1 contains the view of the image that the gallery provides, and in the top part of this window the name of the image is shown. The name of the image shows the date and hour when the image was taken. It cannot be seen in this image, but as the images of this gallery have been processed, the images show the parts of them that are overexposed using white for those pixels and, the parts that are overexposed as a consequence of the postprocessing, with grey pixels. This procedure is quite helpful because very bright zones of the images could have been mistaken with water ice clouds or other water ice formations specially in zones that are over the polar cap.

The green rectangle marked as 2 shows the information about the images that the gallery provides. A brief description of every feature is given in this list:

- Current photo name, Current photo GPID and Time give the date and hour when the image was taken.
- MEX position and MEX distance give the orbital parameters of the spacecraft in the moment when the image was taken.
- Beta gives the angle of the planet that can be seen from the spacecraft
- Exposure gives the exposure time of the image.
- Mouse position allows to navigate the image and gives the location of the planet (latitude and longitude) where the mouse is placed.
- Martian Year provides the Martian Year and Ls gives the areocentric longitude. This is an important parameter because along with the mouse position it can be used to determine the season.
- Current observation name, Current observation GSID, nº (number) photos and Length give information about the observation series.

The yellow rectangle marked as 3 shows two buttons. With the magnifying glass button, it is possible to select the year of the observations and the clock button opens the image that has been selected in the Elkano application.

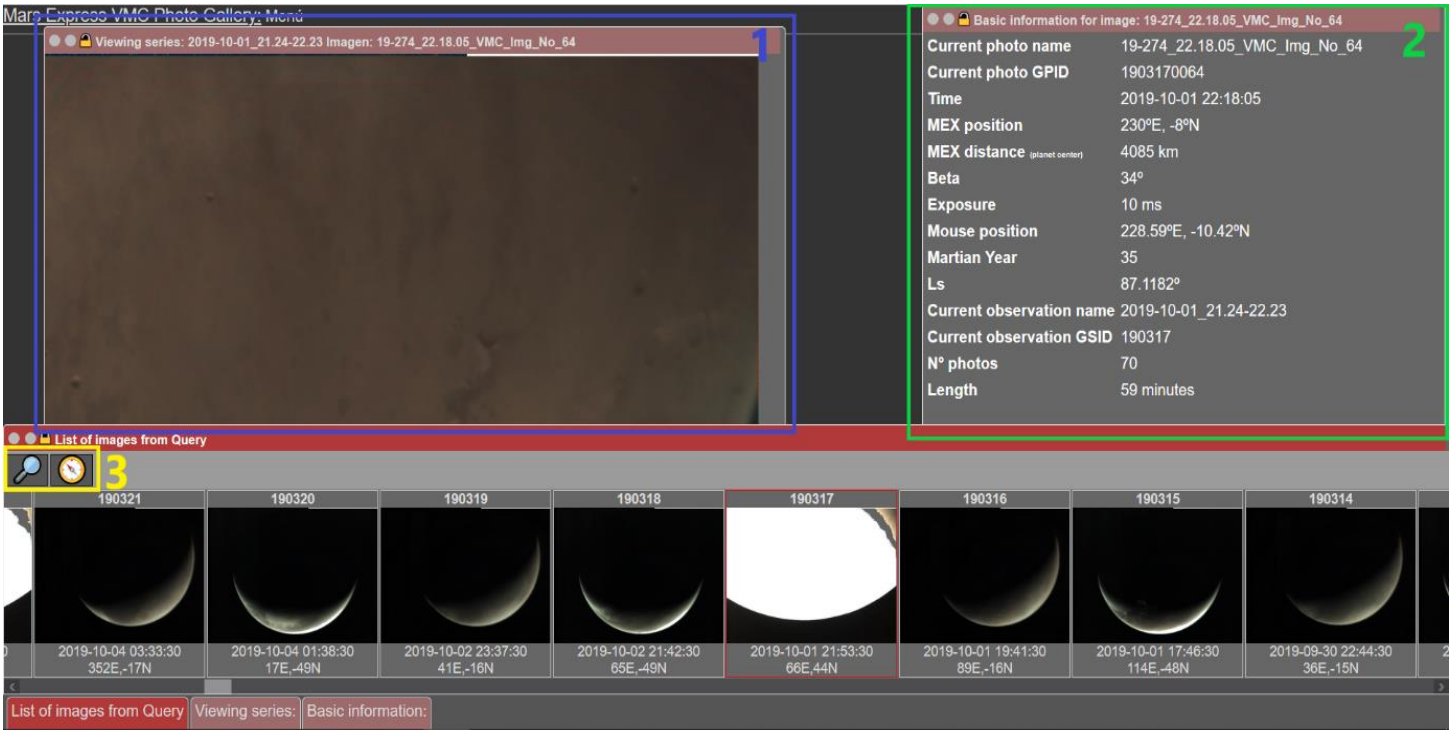


Figure 6. Screenshot of the gallery.

Once the images of interest have been selected, their analysis was made with the Elkano application and to make an accurate and simple description of Elkano a screenshot was taken (Figure 7).

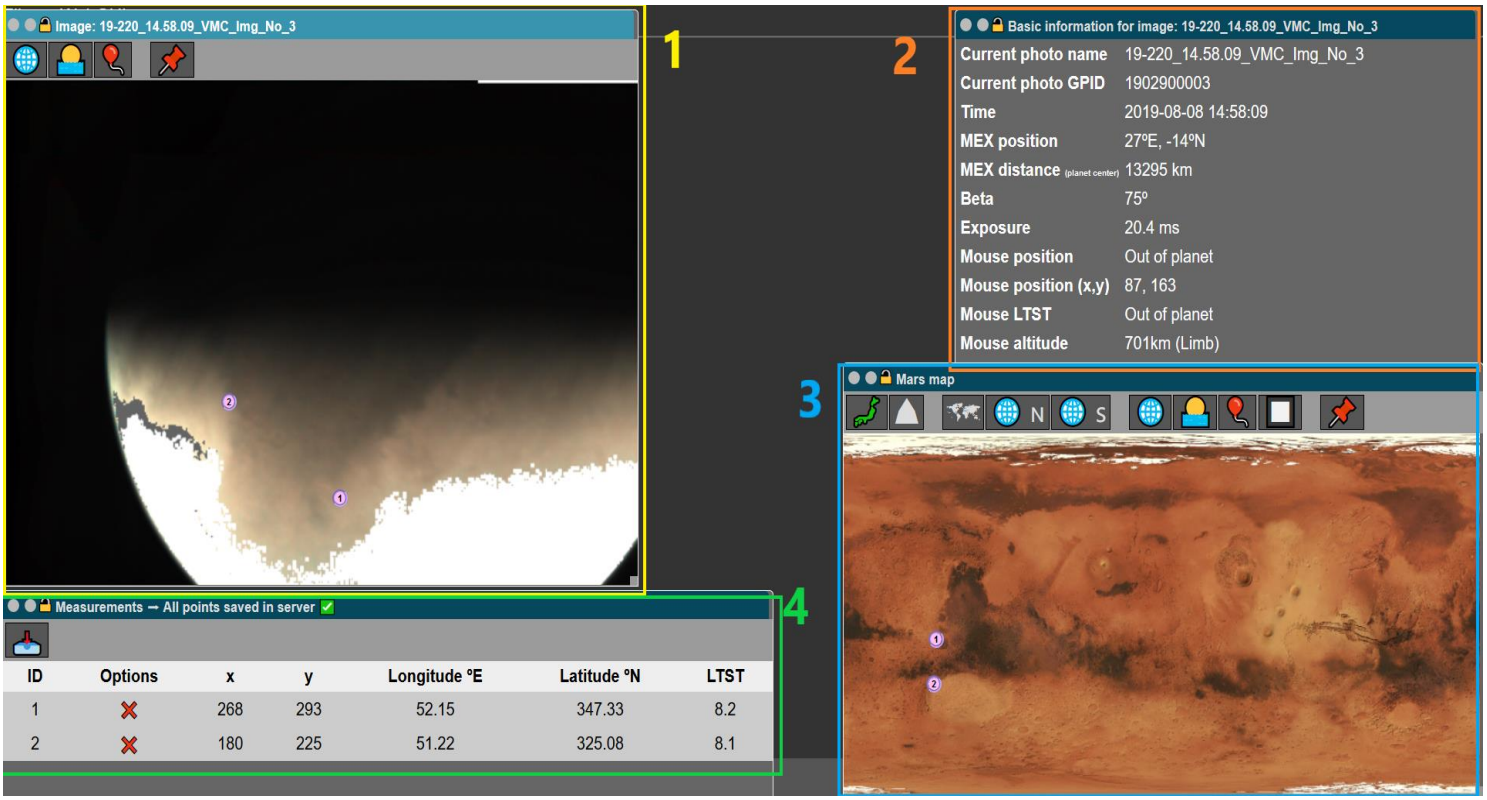


Figure 7. Screenshot of the Elkano application.

As it can be seen in Figure 7, the same method used for the description of the gallery will be followed with Elkano's description. There are 4 different windows in the application and every one of them gives different information about the image that has been selected.

The window in the top-left marked as 1 is the visualization window. In this case, the image that has been chosen shows the feature mentioned before of the coloured (in white or grey) overexposed pixels. This visualization window can be navigated with the mouse as its position in terms of longitude, latitude and height (when the mouse is in the limb) is facilitated in the information window (top-right) at every moment. Whenever a point of the image needs to be marked it is enough with a click and then the marked points are shown in the image as it can be seen in Figure 7. This visualization window has also four buttons (the icons in the top-left part) that allow to show some features (equatorial grid, terminator, limb and the option to hide the marked points) in the selected images.

The window in the top-right marked as 2 is the information window. This window contains the same information shown in the gallery with a few changes. The information of the series is not available here but other characteristics like the mouse position (in terms of pixels with the 0,0 placed in the top-left of the image), the mouse altitude (limb) and the Local True Solar Time (LTST), which is the solar time (hour) of the day, are included here.

The window in the bottom-right marked as 3 is a map of Mars. There are different options in terms of available maps, for example, in Figure 7 an albedo map is shown but a topographic map is also available. A closer look of the polar caps is also available (using the N and S buttons) as a polar projection of both polar caps can be chosen. The other buttons are the same that can be seen in the visualization window with one addition, there is also a button that allows to represent in the map the field of view that can be seen in the selected image. As it happens with the visualization window, the marked points can also be seen in the map along with the mouse position, which is represented with a green dot.

The window in the bottom-left marked in green is the measurement window. The coordinates of the points that have been marked on the visualization window are available here along with the LTST of that point. There is also an option available in this window that enables to delete any marked point, this option is represented by an icon with a red X. The last possibility available in the measurement window is to download the measurements that have been made in a csv file and as a png image. The csv files gather the coordinates and LTST data of the points marked in the images, meanwhile the png images consist in the image that had been opened in Elkano with the marked points, the terminator, the equatorial grid and the limb represented on it.

## 4.2 MEASUREMENT METHODS

Once the structures of interest have been identified and the points of interest in every structure have been marked with the Elkano application it is possible to measure the different properties of those structures. The techniques that have been used in this project to measure the different characteristics of the features are presented in what follows.

### 4.2.1 VMC images

In these images, there are three type of measurements that have been performed depending of the structure that was being studied. This is reported in Table 2.

| ***Table 2*** | | | |
|---|---|---|---|
| ***Structure*** | ***Type of measure*** | | |
| | ***Zonal and meridional size*** | ***Area*** | ***Speed*** |
| Ice clouds/hazes | X | X | - |
| ADS | X | - | In some cases |
| Spirals | X | - | X |
| TDS | X | X | X |

Measuring the zonal and meridional size can be considered as measuring the distance between two different points in the planet's surface. To perform this calculation the procedure stated in [12] was followed. The angular separation between two points 1 and 2 in Mars' surface is given by:

$$\sigma = arcos(sin\varphi_1 \cdot sin\varphi_2 + cos\varphi_1 \cdot cos\varphi_2 \cdot \cos(\lambda_2 - \lambda_1)) \quad (1)$$

- $\varphi_1, \varphi_2$ are the latitudes of points 1 and 2
- $\lambda_1, \lambda_2$ are the longitudes of points 1 and 2
- $\sigma$ is the angular separation

Then, multiplying that angular separation by Mars' radius the distance is obtained. For all the calculations the mean radius of Mars has been used ($R_{Mars}$=3389.5 km).

$$distance = \sigma \cdot R_{Mars} \quad (2)$$

To measure the velocity of the selected features the same procedure was used, but this time the points considered were not part of the same image. First, a selected feature (determined from the shape of a cloud) of the structure was identified in two images of the same series (or in images from different days), then the coordinates of both points were retrieved and, as the Elkano application gives the exact time were the images were taken, the time interval between both measurements is determined.

Dividing the obtained distance by the time interval, the speed of the feature is retrieved.

In the case of the TDS various points were selected in order to see how different zones of the storm were moving, as these structures can cover large parts of the surface and therefore their movement is not uniform.

The last parameter that was measured was the surface that some of these features cover. For the structures that are rather small or have an ellipsoidal shape (some cloud elements, cellular forms of the TDS) the calculation was simply done using the ellipse area.

$$area = \pi \cdot a \cdot b \tag{3}$$

As a and b are the semiaxes of an ellipse, in this case the equation using the length and the width of the structures is simply.

$$area = \pi \cdot \frac{length}{2} \cdot \frac{width}{2} \tag{4}$$

The alternative was to use a program like MATLAB to calculate the area using the coordinates of the points that have been marked in the Elkano application. Introducing the coordinates in MATLAB and using the areaint function, the program returns the part of a sphere (which area is 1) that is covered by the polygon (in this case the feature) that those points form. Multiplying that by the area of the Martian sphere (it was considered a radius $R_{Mars}$=3389.5 km), the surface that the feature covers is retrieved. This alternative has been used to measure the area of the TDS and of some clouds and hazes.

### 4.2.2 HRSC images

Four images from HRSC have been analysed in this project. These images have been processed by the HRSC team showing an integrated grid, as can be seen in Figure 8. However, this grid is not precise enough to measure some of the features (e.g., the size of the cells) of the TDS, therefore, another method was employed.

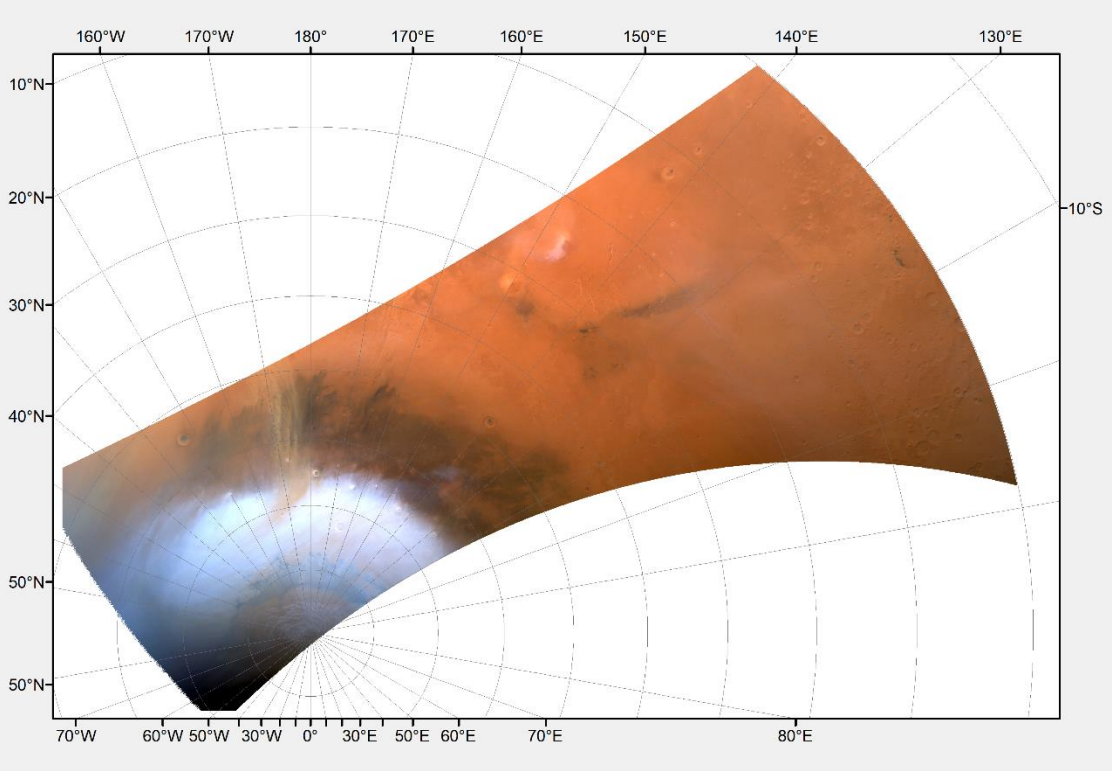


Figure 8. HRSC image with an integrated grid (May 22$^{nd}$, Ls=28.6$^{o}$).

Two different approaches were used and the error of both approaches was considered in order to analyse which one of them was the best. The first approach consisted in using the Korolev crater as a distance scale. First, a line that had the same size of the crater in the image was made, consequently that line would represent the diameter of the crater (in this case 82 km). Later, that line was used as a pattern to measure distances.

To verify the accuracy of this method, the distance between some selected craters that can be seen in Figure 9 has been measured, and then compared with the real distance between those craters. To obtain the distance, the coordinates (latitude and longitude) of those craters have been obtained using JMARS [9] and later they have been introduced in (1). In Figure 9 an example of this method can be seen and in the following tables (Tables 3A-B) the results are presented.

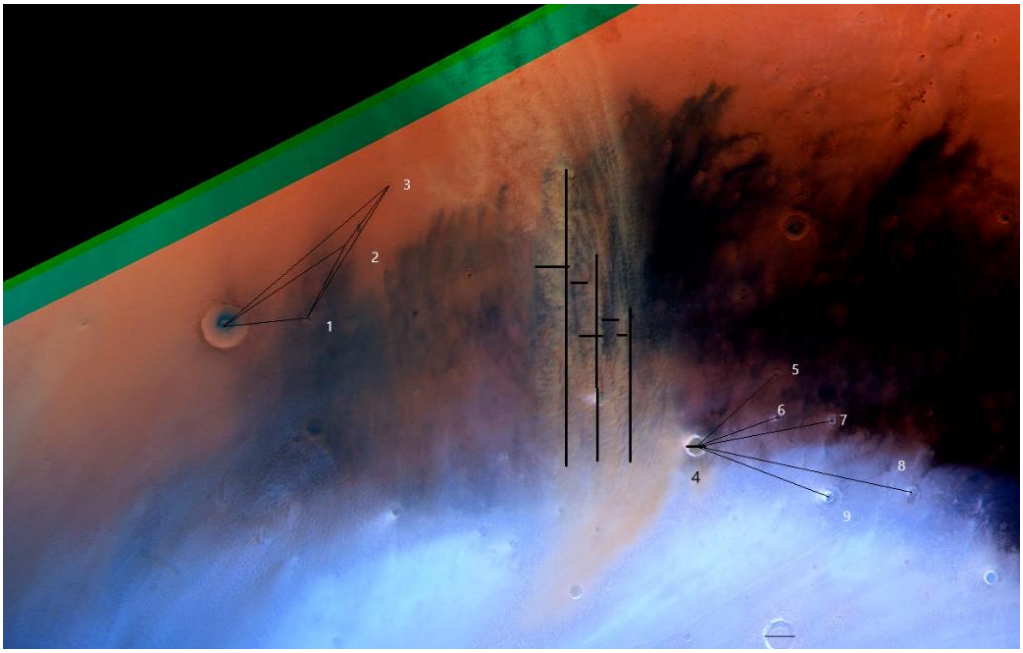


Figure 9. Example of the measurement method using Korolev crater as a pattern [HRSC].

| *Table 3A* | | | |
|---|---|---|---|
| ***Measure*** | ***Real distance (km)*** | ***Measured distance (km)*** | ***Error*** |
| 4-5 | 237.7 | 285.9 | 0.203 |
| 4-6 | 223.7 | 231.3 | 0.033 |
| 4-7 | 356.5 | 370.1 | 0.037 |
| 4-8 | 555.1 | 592.9 | 0.068 |
| 4-9 | 362.4 | 382.6 | 0.055 |

In table 3B, the M stands for Milankovic crater, which can be seen in the left part of Figure 9 and it has been used in the measures.

| *Table 3B* | | | |
|---|---|---|---|
| ***Measure*** | ***Real distance (km)*** | ***Measured distance (km)*** | ***Error*** |
| M-1 | 194.1 | 222.9 | 0.148 |
| M-2 | 323.1 | 391.1 | 0.211 |
| M-3 | 528.5 | 580.3 | 0.097 |
| 1-2 | 180.5 | 222.9 | 0.238 |
| 2-3 | 213.7 | 201.8 | 0.055 |
| 1-3 | 391.8 | 416.3 | 0.062 |

Using this method an **11% mean error** is obtained. This was considered to high so a shift to another method was made.

This second method consisted in measuring the km/pixel ratio of the images using a free image editor software, in this case GIMP [w5]. This program has a tool that allows to measure the pixels between two points of the image, therefore if the real distance of those points is known, the km/pixel ratio of the image can be found.

In order to apply this method a reference must be stablished and the one used in this example was the Milankovic crater. The first step was to choose two points of the crater that could be easily recognized in both images (JMARS' atlas and HRSC's images). After that, the real distance of these points was calculated using the coordinates of both points (A and B). The chosen points can be seen in Figure 10.

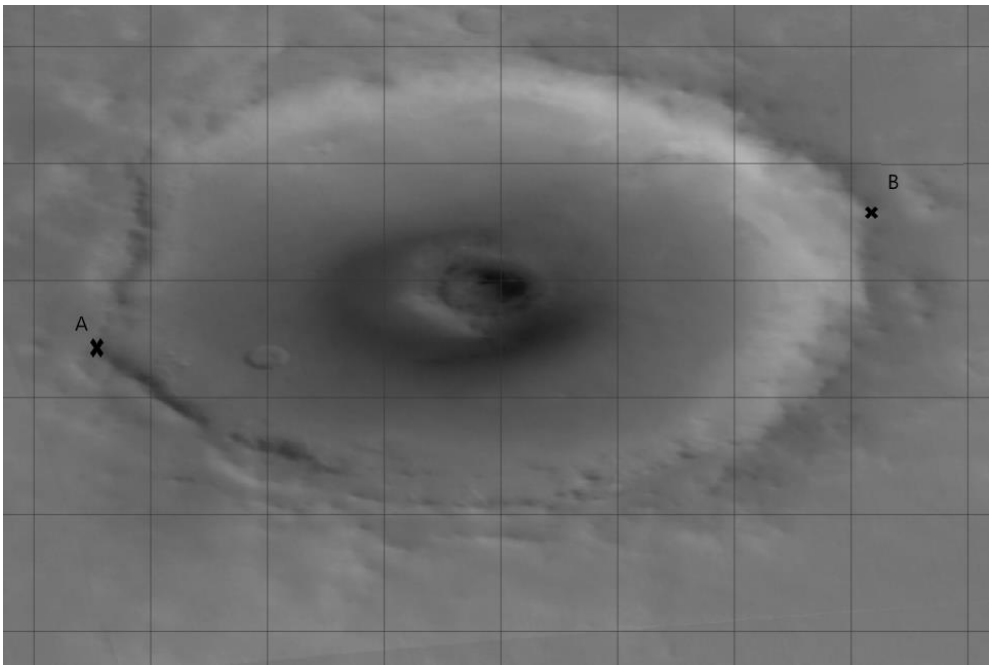


Figure 10. Milankovic crater used as reference [JMARS].

Once the real distance of those points was known, the distance (in terms of pixels) was measured in the HRSC's images using GIMP. Thus, the km/pixel ratio of the images was found and a new comparison between the real and the measured distance was made using the same craters marked in Figure 9. The results can be checked in the Tables 4A-B.

| ***Table 4A*** | | | |
|---|---|---|---|
| ***Craters near Milankovic*** | | | |
| Measure | Real (km) | Measured distance (km) | Error |
| M-1 | 205.9 | 202.1 | 0.018 |
| M-2 | 346.3 | 356.1 | 0.028 |
| M-3 | 515.5 | 531.2 | 0.031 |
| 1-2 | 189.6 | 200.9 | 0.059 |
| 2-3 | 179.9 | 179.3 | 0.003 |
| 1-3 | 377.8 | 383.8 | 0.015 |

| ***Table 4B*** | | | |
|---|---|---|---|
| ***Crater 4 area*** | | | |
| Measure | Real (km) | Measured distance (km) | Error |
| 4-5 | 270.9 | 263.9 | 0.025 |
| 4-6 | 219.8 | 212.8 | 0.031 |
| 4-7 | 349.1 | 339.1 | 0.028 |
| 4-8 | 558.7 | 544.1 | 0.026 |
| 4-9 | 359.4 | 348.6 | 0.031 |

Using this method, the error reduces to **2.7%**.

This method was applied in two of the HRSC's images (those with TDS) and the mean error was calculated for those images. In Table 4C the km/pixel ratio of the images and the mean error are presented.

| ***Table 4C*** | | |
|---|---|---|
| ***Image*** | ***km/pixel*** | ***Error*** |
| May 22 | 2.07 | 2.7% |
| May 26 | 1.487 | 2.2% |

This method was not used in the other two HRSC's images because the features (clouds, ADS) that can be seen in those images are easily analysed using the integrated grid from the HRSC team. Furthermore, this grid was also useful to obtain the coordinates utilized to measure the area of the TDS with the method mentioned in section 4.2.1 and to measure the size of other formations with the procedure described in (1) and (2).

## 4.3 THEORETICAL METHODS

The methodology followed in the theoretical analysis required of two different tools JMARS and the MCD. JMARS (stands for Java Mission-planning and Analysis for Remote Sensing) is a public software that provides data-analysis tools for scientist or the general public [9]. In the case of this project JMARS has been used to represent the different observed phenomena over a map of the Martian surface. This representation helps to understand which regions show more activity and that will be useful at the time of selecting the regions that need to be analysed with the MCD.

The MCD [10 & 11] is a database with a lot of different possibilities in terms of analysis of the Martian atmosphere, as it provides a realistic model of the Martian atmosphere based on General Circulation Model (GCM) numerical simulations and the observational data gathered by the different missions that have been in the red planet.

The objective of using the MCD is to establish a comparison between the observations of dynamical phenomena and the predictions proportionated by the MCD. A way to establish this comparison is to measure different variables of the Martian atmosphere that are related to the observed phenomena. The selected variables to study the different phenomena are listed below:

- Water ice mixing ratio and water ice column (water ice hazes/clouds).
- Dust mass mixing ratio and dust column visible optical depth for dust events.
- Zonal, meridional and vertical wind for comparison with the measured speeds and for an evaluation of the atmospheric stability.
- Temperature for atmospheric stability and surface wind stress for dust events.

Focusing the attention on the surface wind stress [13], this is a variable that can shed light on which zones are more active in terms of dust lifting and therefore initiating processes that may end up developing the observed dust formations. This surface wind stress is related to the saltation process [14], whose mechanism consists in wind strong enough to lift dust particles which will described a parabolical movement ending up in the surface again, causing an impact that will lift thinner dust particles to the atmosphere. The value of the surface wind stress that has been considered as sufficient to mark a determined zone as active lies in the range of 0.01 – 0.06 Pa as it is stated in [15]. The other processes acknowledged as dust lifting processes are the dust devils but in this project this type of mechanism has not been studied.

Once the different variables have been clarified it is time to determine the zones and the periods of time that are going to be studied. The following considerations have been made:

- As the project is focused in the north polar region, the range of latitudes considered is $30^{o}$ N - $90^{o}$ N.
- All longitudes are taken into account.
- The studied height range goes from the surface to 20 km.

- Two hours of the Martian day were considered, 0h and 12h. This is intended to cover a broad margin in time for variability of the atmospheric conditions but as all the images were taken during the day, 12h was used as reference.
- This project is focused on the spring of the northern hemisphere (Ls $0^o$ - Ls $90^o$), therefore four different periods of time have been selected (Ls $0^o$, Ls $30^o$, Ls $45^o$, Ls $90^o$).
- In order to obtain a better precision, the high-resolution topography option has been selected.

MCD has gathered data from MY 24 to MY 31 and can create scenarios taking into account the data from that period. This option is called the dust/EUV scenario, where EUV refers to Extreme Ultra-Violet input and it is conditioned by the solar cycle and on the other hand, the dust scenario takes into account the amount and distribution of suspended dust in the atmosphere, which is important as dust has a major influence in the atmospheric dynamics. There are two scenarios that might be suitable to the case of study, these are cold (low dust, min solar) and climatology min solar.

The cold scenario considers a clear (low dust) and cold atmosphere and sets dust relate variables to the minimum observed in the period mentioned before. This has been considered as inadequate for this project because there is no data available to make the suggestion that the spring of MY 35 fits the cold scenario. Therefore, the climatology min solar scenario has been chosen as is well known the solar cycle was in its minimum in that time of 2019.

Once all the options have been set the data can be downloaded and the comparison can be made. The downloaded data has also served to make a deeper study of the three different spirals that have been identified during this project as a baroclinic study of all three of them has been made using data obtained from the MCD.

# 5. RESULTS AND THEIR ANALYSIS

In this part, the different structures that have been identified will be described along the results of the theoretical analysis. The images shown in this section were either taken by VMC and HRSC or made using tools like JMARS and MCD.

## 5.1 IDENTIFIED STRUCTURES

The identified structures can be divided in two different groups, the water ice formations (hazes, clouds and one of the spirals) and the dust structures (TDS, ADS and other kind of diffuse structures). As it has been pointed out, all these formations formed in the north polar region of Mars during the northern spring (Ls $0^o$ - $90^o$). After a quick overview, it can be determined that the most common meteorological formations were clouds and ADS. This can be seen in Figure 11 were all the identified structures were placed over a map using JMARS, from data gathered by the Mars Global Surveyor (MGS) spacecraft using the Mars Orbiter Laser Altimeter (MOLA).

The map has a colour code, which is placed in the lower part of the image, in order to facilitate the identification of the different formations. A few clarifications must be made regarding this map:

- The location of the limits of the polar cap were measured using images of VMC and the date (in this case expressed as Ls) marked in both cases, corresponds to the first and the last observed features.
- There are two types of clouds in the map. The ones shaped as lines are considered as thin clouds with a width ~ 150-200 km. The ones shaped as polygons are bigger and their area has been measured.
- There are two types of dust features in the map. The ones shaped as lines are considered ADS with a width ~ 80-125 km. The ones shaped as polygons are formations of thin dust or scattered dust with only one exception that will be presented later. In those cases the area has been measured.

Based on what can be seen in the map of Figure 11, the regions with a major activity can be identified. In terms of latitude the zone between latitudes $50^oN$ - $75^oN$ shows the biggest activity. It can be also seen that there is almost no activity in latitudes above $80^oN$. It must be pointed out that there are no phenomena reported in latitudes below $40^o$ N because it was considered as a zone that it lies too far from the polar cap.

In terms of longitude, most of the phenomena are located between $180^oE$ – $340^oE$ and there are zones were no phenomena has been observed. These zones are rather small in the range of longitudes $35^oE$ - $65^oE$ and $115^oE$ - $130^oE$.

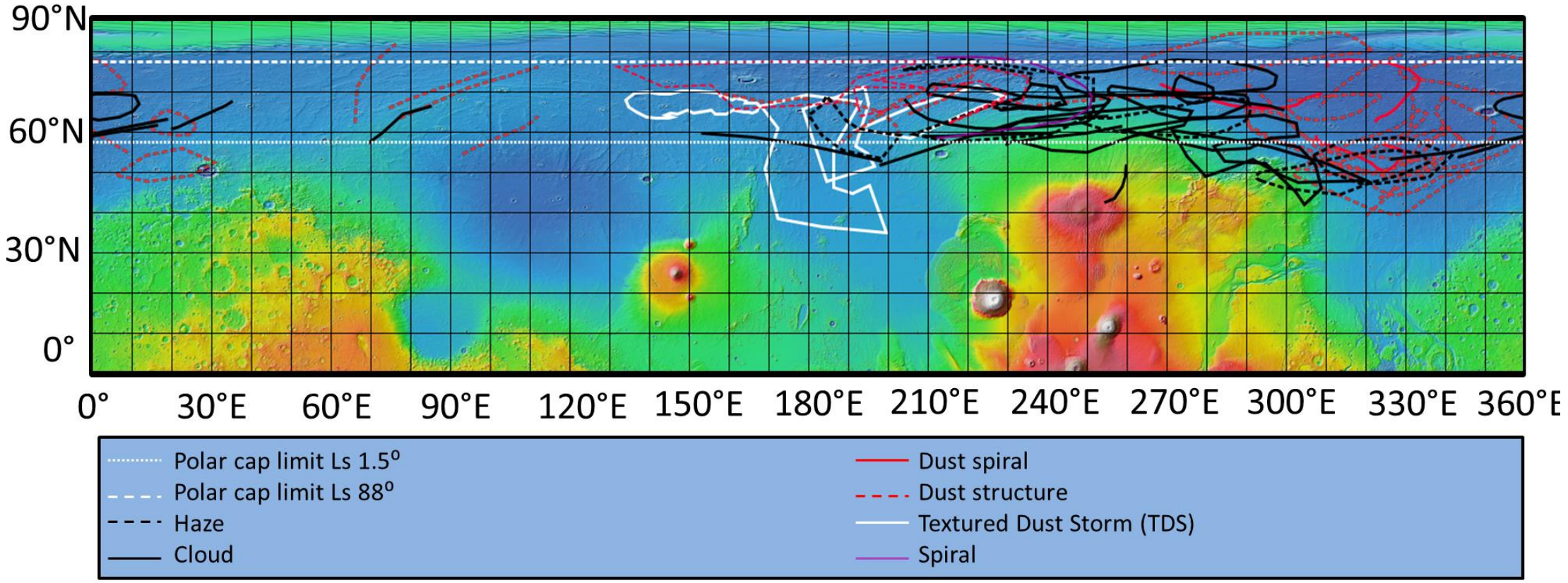


Figure 11. Identified structures [JMARS].

## 5.2 CLOUDS AND HAZES

Clouds and hazes are distinguished from dust by their white colour when compared with the yellowish one shown by dust. Clouds are identified by their high reflectivity and density whereas hazes are thinner, sometimes transparent, formed by water ice condensates. Between these two water ice formations, based on what has been seen in the observations, clouds are more common. However, there might be an observational bias as the hazes are more difficult to observe in the VMC's images due to the technical constraints of the instrument, particularly if the haze is very thin. It has been considered that all of these structures are water ice based on the temperature data obtained from MCD. This is shown in Figure 12, where in the top the temperatures of a particular moment (considered as one of the coldest of the observation window) are shown. This is an attempt to make a quick comparison between the temperatures in the spring season of Mars and the temperatures (Figure 12, bottom) that are necessary for $CO_2$ to condensate. It has been considered that the temperatures in the regions where the clouds have been observed (55ºN - 60ºN, ~ 175 K) are high enough to avoid the formation of $CO_2$ clouds.

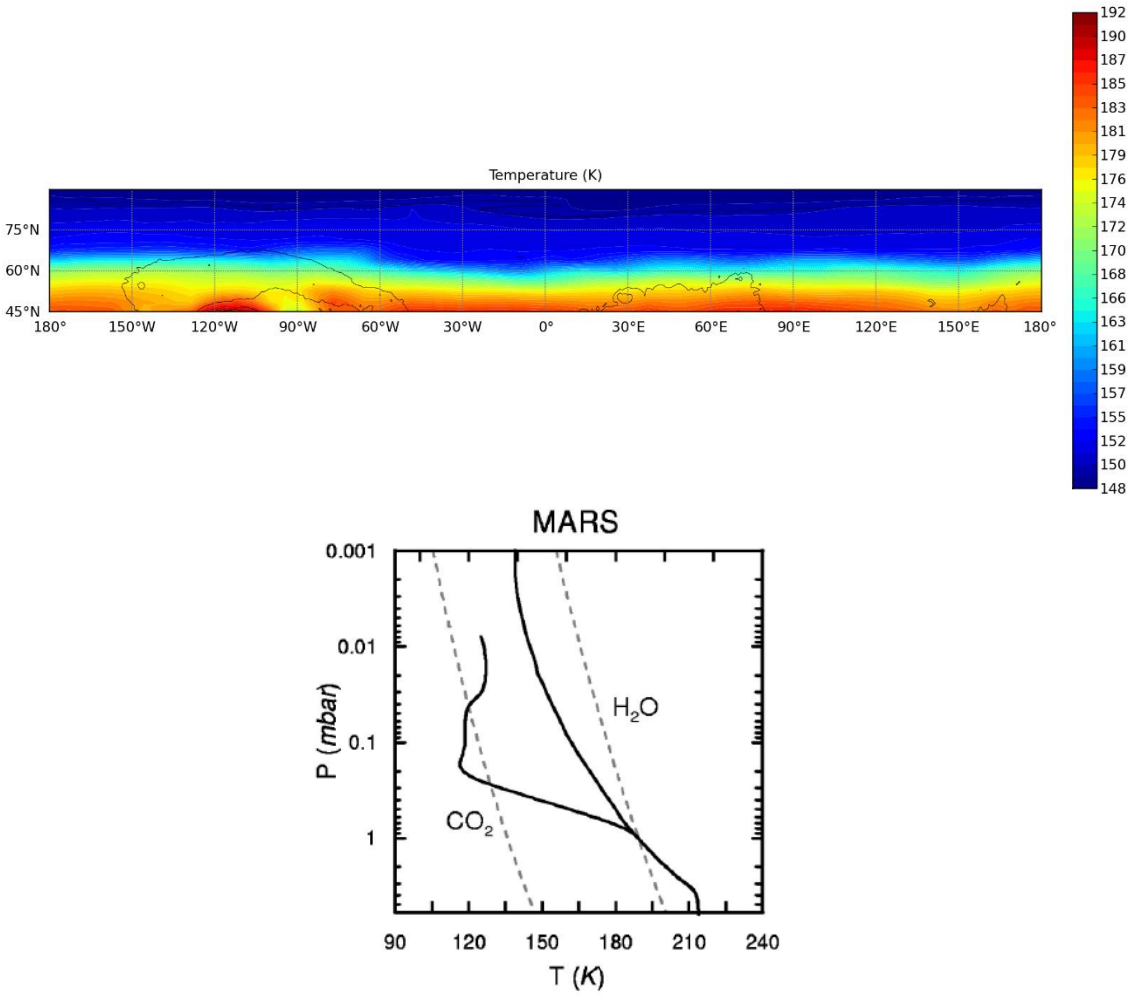


Figure 12. Temperatures in Ls=0º, 8h at Z=10 km (top, obtained from MCD) compared to saturation vapor pressure curve (dashed lines) of $H_2O$ and $CO_2$ [16].

Once it is settled that these formations are composed by water ice a difference between them must be established. As indicated above classifying a feature as haze or cloud is based on the optical depth of the structure. If the structure is thick enough to avoid the surface from being seen it is considered as a cloud, on the other hand, if the surface can still be seen under the condensate is classified as a haze. An example is shown in Figure 13.

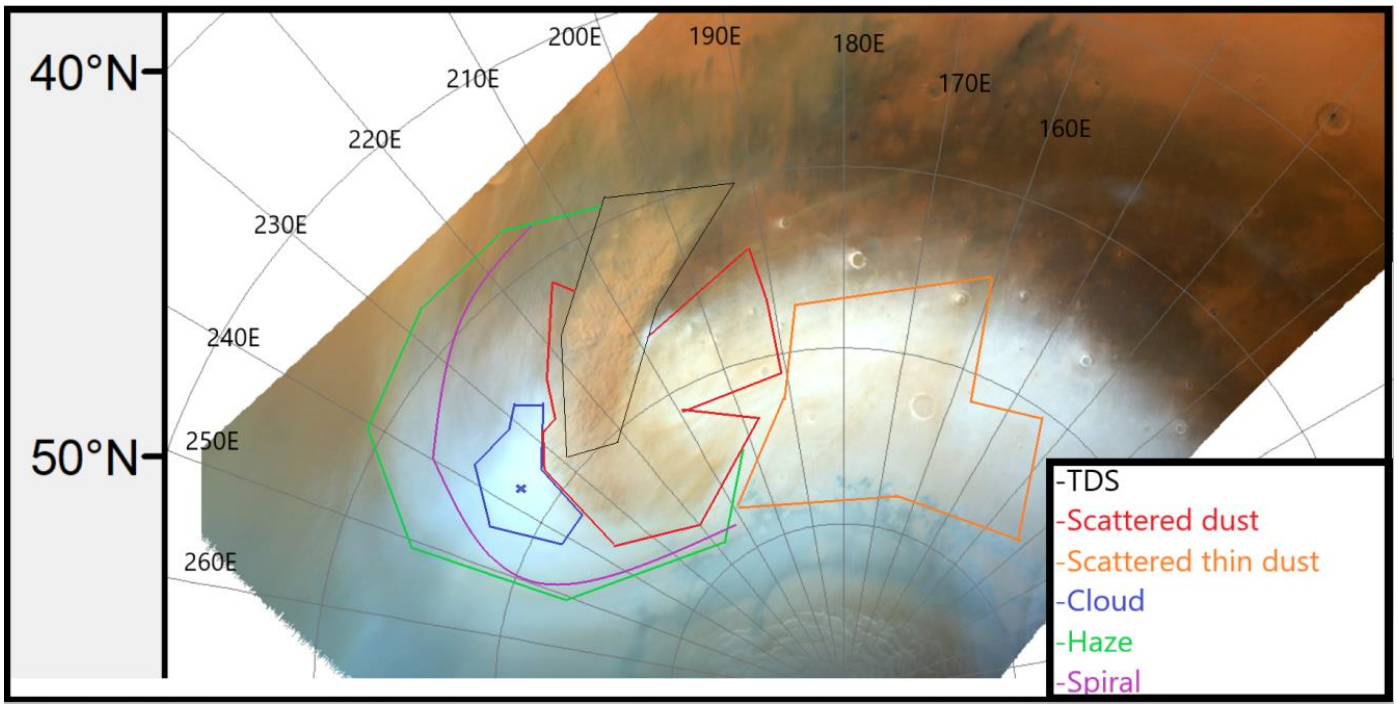


Figure 13. Cloud and haze seen by HRSC in May 26th (Ls=30.4º).

The haze, whose limits are marked by the green line, allows to see some features of the Martian surface. The cloud, by contrast, covers the surface beneath and due to the fact that it is bright and opaque, the limits of the polar cap cannot be seen.

A map (Figure 14, top) with the water ice structures has been created using JMARS to help with the identification of zones that show this kind of structures. According to the observations, the range of longitudes 200ºE - 320ºE is the most active while from 90ºE - 150ºE no activity at all was seen.

In terms of latitude, all these structures have been observed in the 50ºN - 80ºN strip and the evolution during the spring in terms of their location can be noted (Figure 14, bottom). From that, it can be observed that these formations move north as summer gets close, following the retreat of the polar cap. This happens because it is necessary that the atmosphere is cold enough for the $H_2O$ to condensate and these only happens in latitudes that are either covered by the polar cap or close to it.

The last cloud was spotted in Ls=53º but this could be produced by an observational bias as there were less images of the north polar region from VMC in the period of time Ls = 53º - 90º.

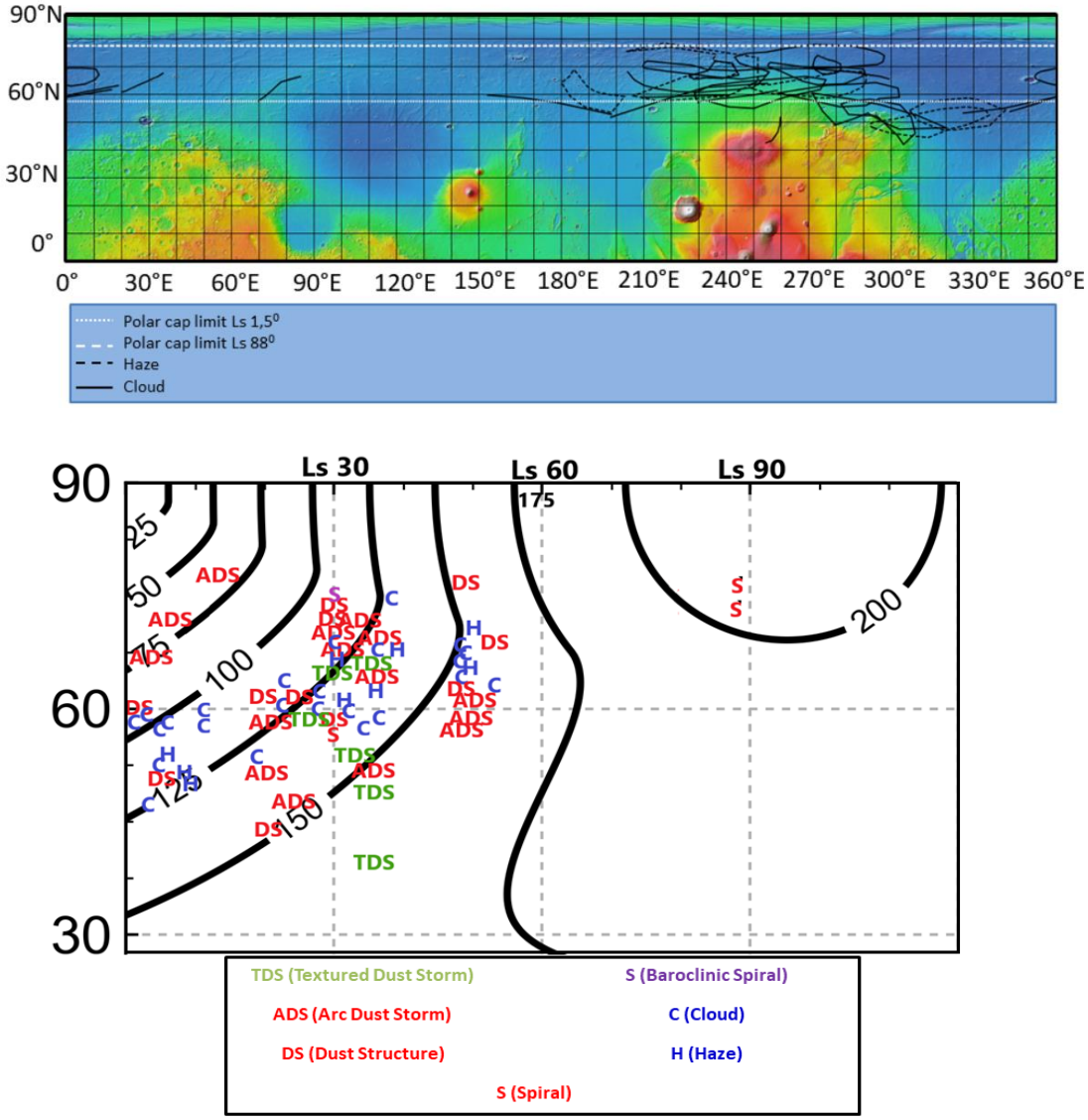


Figure 14. Surface map (top, from JMARS) with the location of the water ice structures and insolation map (bottom, units in $Wm^{-2}$) with the structures placed according to their latitude and date (Ls).

In Table 5 the main characteristics of the water ice condensate formations are given.

| ***Table 5*** | | | |
|---|---|---|---|
| ***Structure*** | ***Mean length (km)*** | ***Mean width (km)*** | ***Mean area ($km^2$)*** |
| Thin clouds | ~ 800-900 | ~ 150-200 | – |
| Clouds | ~ 1200 | ~ 350 | $3.3 \cdot 10^5$ |
| Hazes | ~ 1300 | ~ 450 | $4.7 \cdot 10^5$ |

In order to study the formation of water ice clouds in the north polar region of the planet the MCD has been used to get maps of the water ice column (kg/m$^2$) and the water ice mixing ratio. Two of the considered periods of time (Ls 60$^o$ and Ls 90$^o$) were not be taken into account because the last cloud was observed in Ls 53$^o$. After generating the maps for the other Ls, it was found that the clouds and hazes tend to form where the water ice column and water ice mixing ratio show a larger meridional gradient in their values. Figure 15 shows a map of the water ice abundance for Ls = 30$^o$ and 20 km height. Superimposed on it are the clouds (C) and the hazes (H) that have been identified in the images.

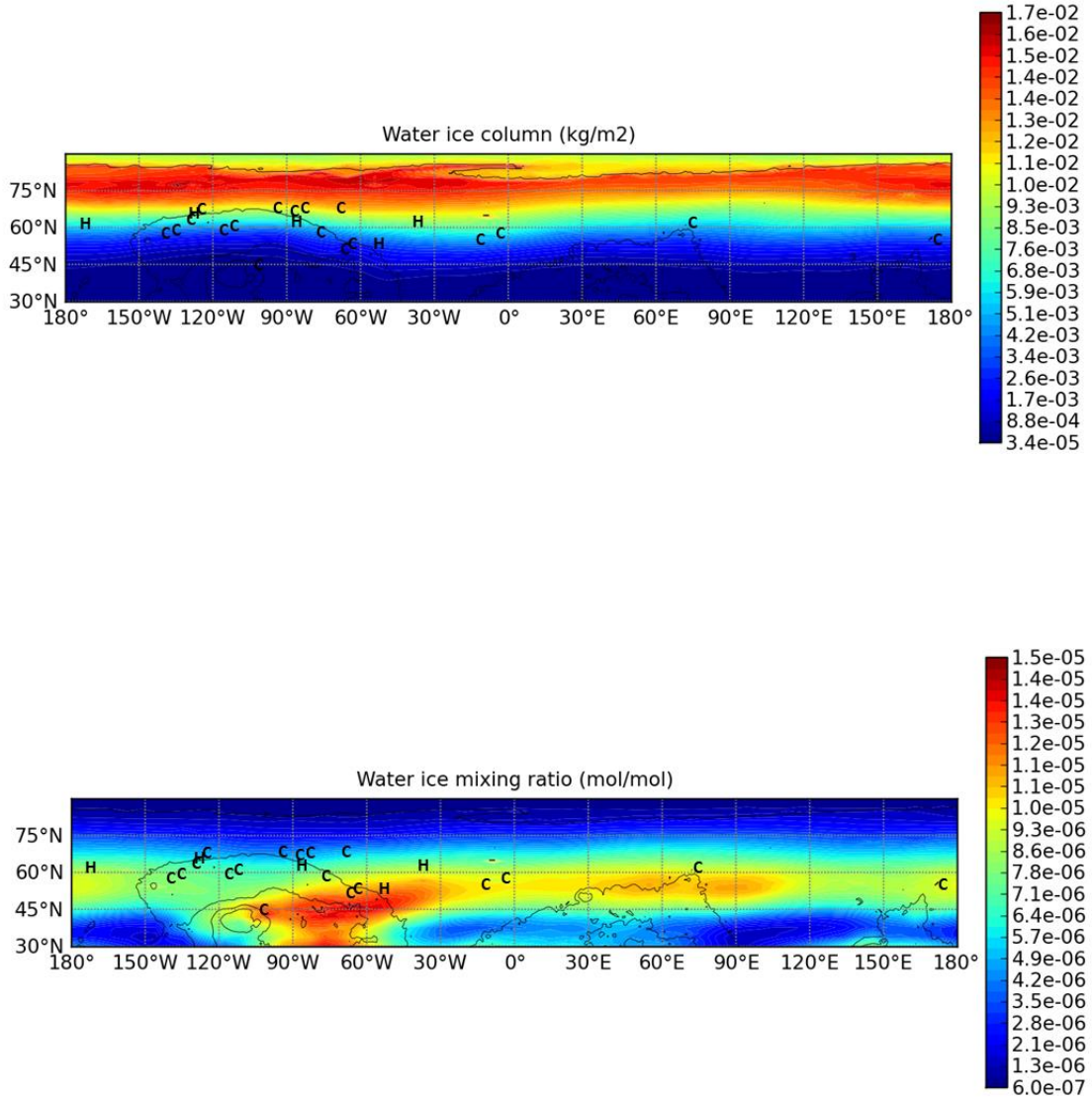


Figure 15. Comparison between MCD's data (Ls=30$^o$, 12h Z=20 km) and observations [MCD].

The MCD data reflects the biggest concentration of water ice (in terms of mixing ratio) in the range of longitudes 260$^o$E - 320$^o$E and that coincides with the observations. Another thing that agrees with the results of the observations is that in the MCD the zones of large concentration of water ice move towards north as summer's solstice gets close and this can be compared with Figure 14 (bottom).

## 5.3 ARC DUST STORMS AND OTHER DUST STRUCTURES

In this section some of the dynamical features that are composed by dust are presented, while the other two features, TDS and spirals, will be addressed later separately. The dust structures have been identified as areas of thin dust, as the surface that is beneath them is still visible. An example of all the dust features is shown in Figure 17, in that figure the first image shows an ADS, the second image shows a spiral with areas of diffused dust over the polar cap and the third and fourth image show a TDS and a spiral respectively.

Only a few of those diffused dust structures have been identified but this is due to an observational bias, as it happened with the hazes. Due to the characteristics of these structures visible by the thin scattered dust, they are not easy to identify using VMC, in fact, most of these structures have been spotted in HRSC's images. This is shown in Figure 16, where there are more ADS (dashed lines) than dust structures (dashed polygons).

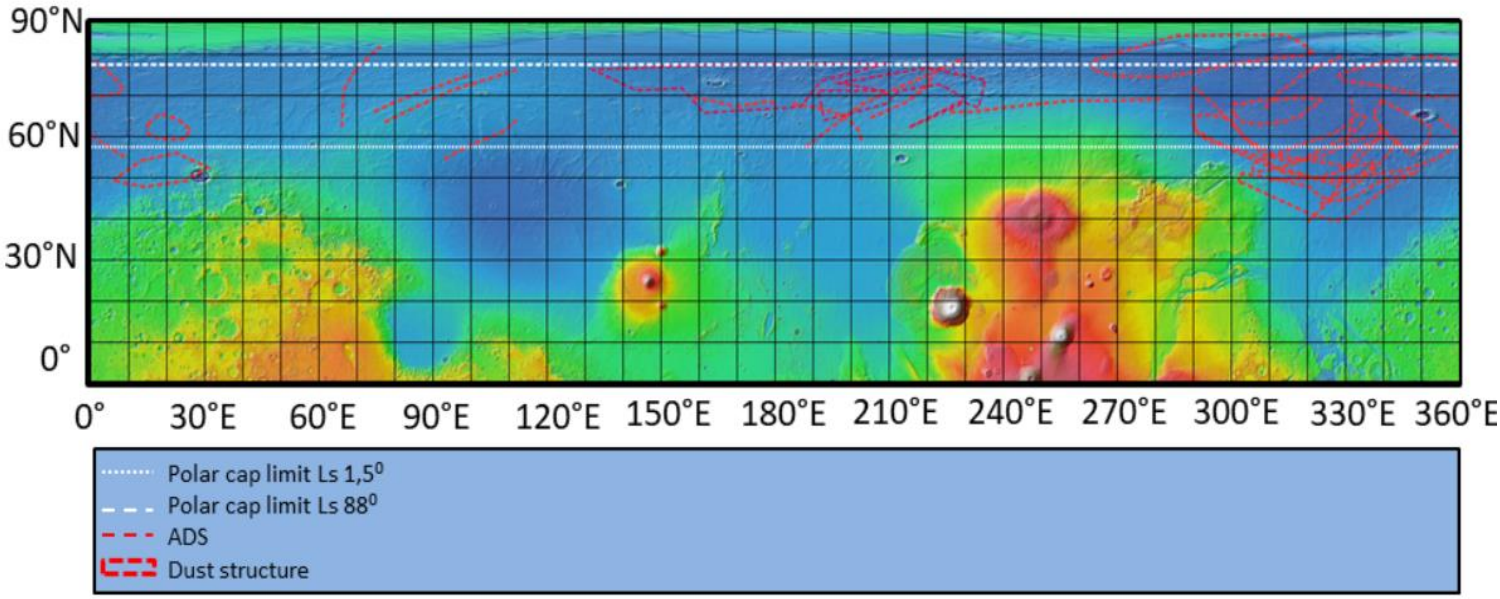


Figure 16. Map of Mars with the ADS and the dust features represented on it [JMARS].

The other type of structure studied in this section are the ADS. This name responds to their shape, because all of these structures have a characteristic arc-shape morphology. In previous works [17 & 18] this kind of structures are also named as frontal dust storm and upon expanding they are classified as a flushing dust storm (from now on FDS). The FDS are originated in the edge of the polar vortex and move southward through certain areas, which according to [17] are the Planitias of Arcadia, Acidalia and Utopia. In some cases, these storms transport dust to the southern hemisphere but as they are moving south, they start to lose their characteristic shape. This kind of phenomena have their peak [18] during the northern fall and winter.

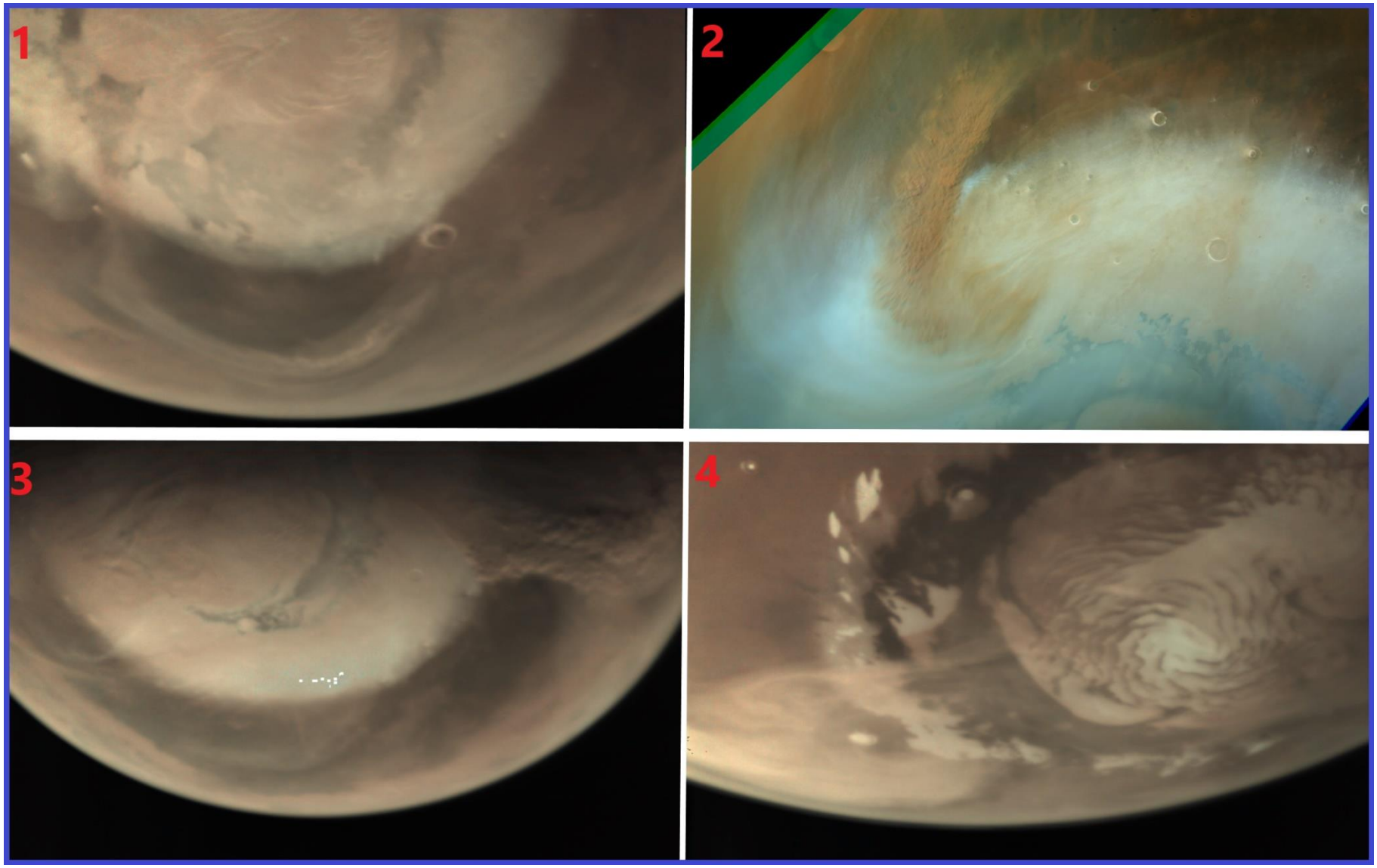


Figure 17. The four different dust features that have been identified: ADS (1), dust structure (2), TDS (3) and spiral (4) [VMC & HRSC].

Because there are not sufficient images to measure the dust arcs' evolution (most probably a southward expansion), their classification has been maintained as ADS rather than FDS.

It is not possible to measure their speed because as a consequence of their size and VMC's capabilities, it has not been possible to identify similar features of the structures in different images and hence, the mentioned method which has been used to measure other structures' speed cannot be applied. Only in one particular case it has been possible to measure the speed of an ADS and therefore a complete analysis (which will be reported later) of the structure has been made. In Figure 18 a clear example of an ADS is presented and it can be seen that is quite difficult to distinguish features within it.

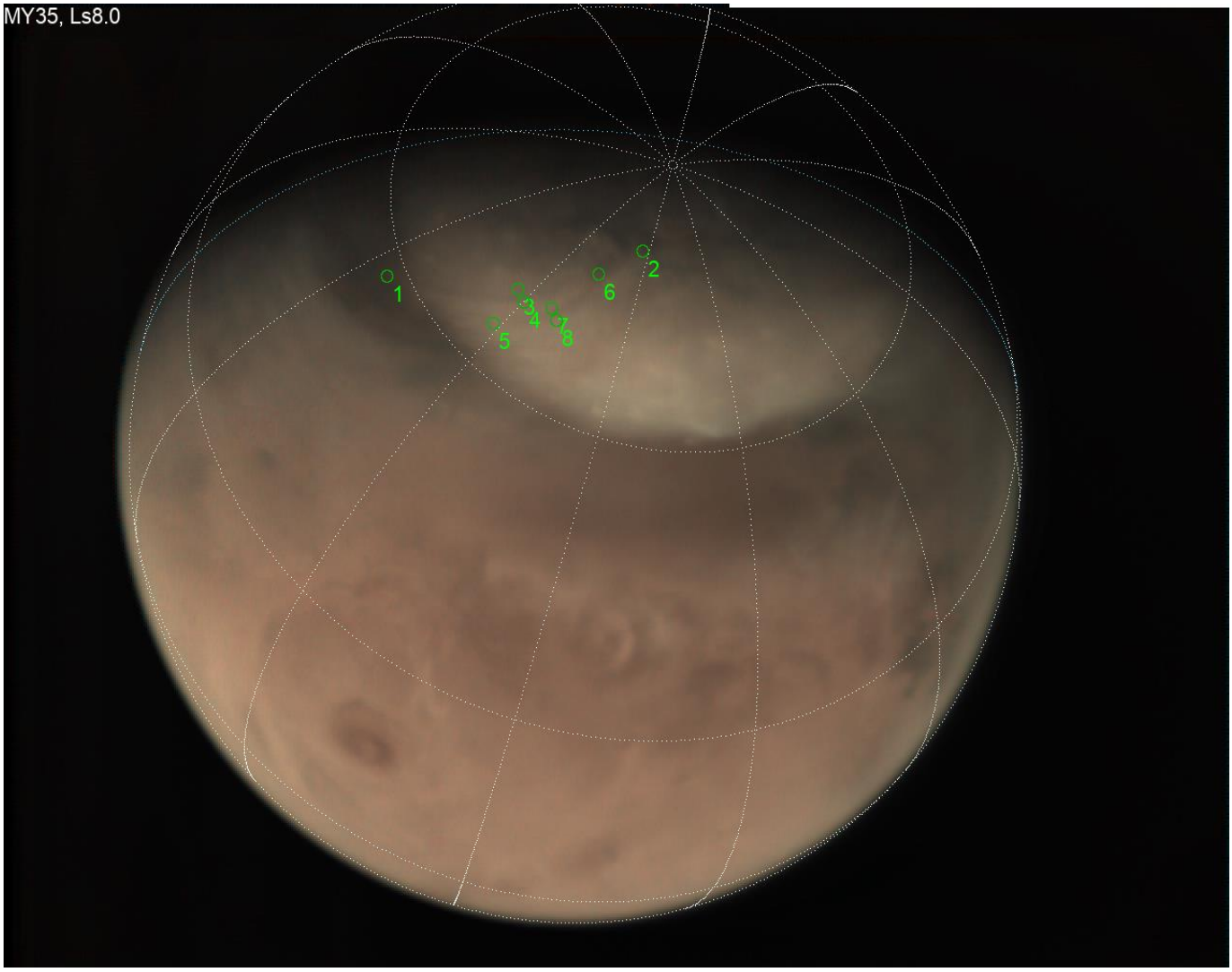


Figure 18. Double ADS over the polar cap April 8th (Ls=8º) [VMC].

Looking back to the map of Figure 16 there are zones with more activity, as 290ºE - 350ºE near Acidalia Planitia and in 190ºE - 230ºE near Arcadia Planitia. These areas show high activity as reported in [17 & 18] for the FDS with the exception of the Utopia Planitia where almost no activity was spotted.

As for the study of the water ice structures, since Ls=53º onwards almost there were no good images of the northern polar region provided by VMC. This can be seen in Figure 14 (bottom) and it can be also assessed from that figure that the locations of the ADS and the dust structures do not follow the tendency reported for the water ice features. The area of the dust structures has been measured and for the ADS the mean length and width has been measured. This can be seen in Table 6.

| ***Table 6*** | | | |
|---|---|---|---|
| ***Structure*** | ***Mean length (km)*** | ***Mean width (km)*** | ***Mean area (km²)*** |
| Dust structure | - | - | $2.9 \cdot 10^5$ |
| ADS | ~ 1000-1200 | ~ 80-125 | - |

A deeper study of one of the ADS over Acidalia Planitia has been conducted due to the availability of series of VMC images, measuring their properties with detail (size and velocity). This ADS (Figure 19) was observed in the edge of the polar cap in Ls=50º and its exact location was between 300ºE - 330ºE which coincides with one of the corridors were the FDS are observed to move southwards.

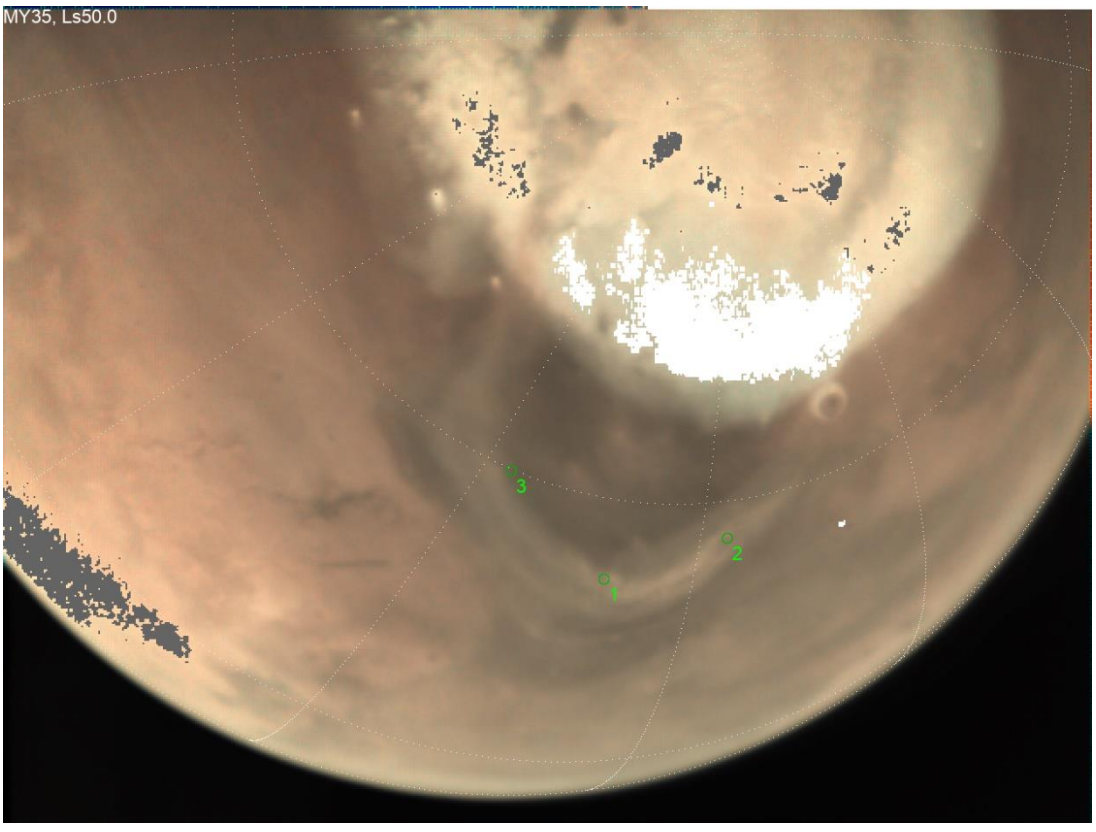


Figure 19. ADS spotted in July 9th (Ls=50º) over the Acidalia Planitia [VMC].

This ADS is the biggest one that has been observed, it is ~2350 km long and ~250 km wide. It started right over the edge of the polar cap and it extended southwards. Three points have been considered to measure its speed but one of them (point 3) gave no good results because it was not possible to locate it in the other images with enough precision. A mean speed of 29 $ms^{-1}$ is retrieved, but after looking at the locations of the points (Table 7) it is certain that this ADS is moving northwards, therefore it cannot be classified as an FDS.

| ***Table 7*** | | |
|---|---|---|
| ***Image*** | ***Latitude point 1*** | ***Latitude point 2*** |
| 1 | 53.62º | 56.97º |
| 2 | 53.93º | 57.04º |
| 3 | 54.23º | 57.27º |

Using MCD's data it is possible to constrain the height of the ADS. This can be done by comparing the measured speed with the horizontal wind speed predicted by the MCD (Figure 20) in that zone in that time of the year and for different heights. The approximate location of the structure is marked in the map with de ADS letters. In that location MCD predicts at Z=10 km a horizontal wind speed of ~ 25 $ms^{-1}$, which is close enough to the measured value. However, this approximation can be inaccurate because the speed that has been measured for the ADS is the radial speed of its expansion but as the MCD gives the horizontal wind speed it has been considered acceptable to use this parameter for the comparison.

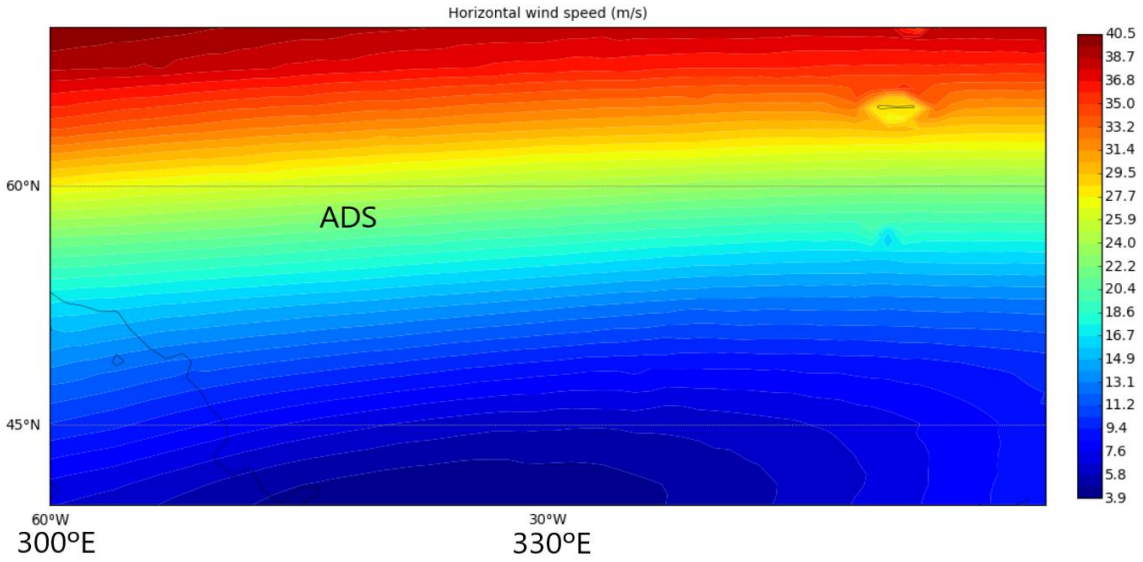


Figure 20. Horizontal wind speed in Ls=50º at 12h and 10 km height [MCD].

The other comparison with MCD involves the dust mass mixing ratio, the dust column expressed as visible optical depth and the surface wind stress predicted by the model. The data downloaded for Ls=90º was not taken into account as there were no ADS or dust structures spotted near that period of time and it has been taken as reference for the dust abundance in the area the altitude of 10 m, the minimum altitude allowed by the MCD.

Meanwhile, there is no problem in that aspect with the visible optical depth because that parameter does not change with the height. Besides, the presence of dust at that height (close to the surface) indicates zones that have a bigger chance to develop major dust phenomena like the ones that have been observed.

After placing the observed phenomena over the maps (for different Ls) the conditions of the atmosphere at Ls=45$^{o}$ (mid-spring) were the ones that presented the best choice to explain the observations. According to MCD the biggest accumulations of dust and therefore, the zones with a higher chance for dust to be updrafted by ambient winds are in the 280$^{o}$E - 360$^{o}$E longitude range (Figure 21). That zone is where more ADS and dust structures were reported and is eastwards of this zone that has more chances to present a notable dust lifting due to the higher values of the surface wind stress, which are 0.01 – 0.02 Pa, suitable for dust lifting conditions as stated in [15].

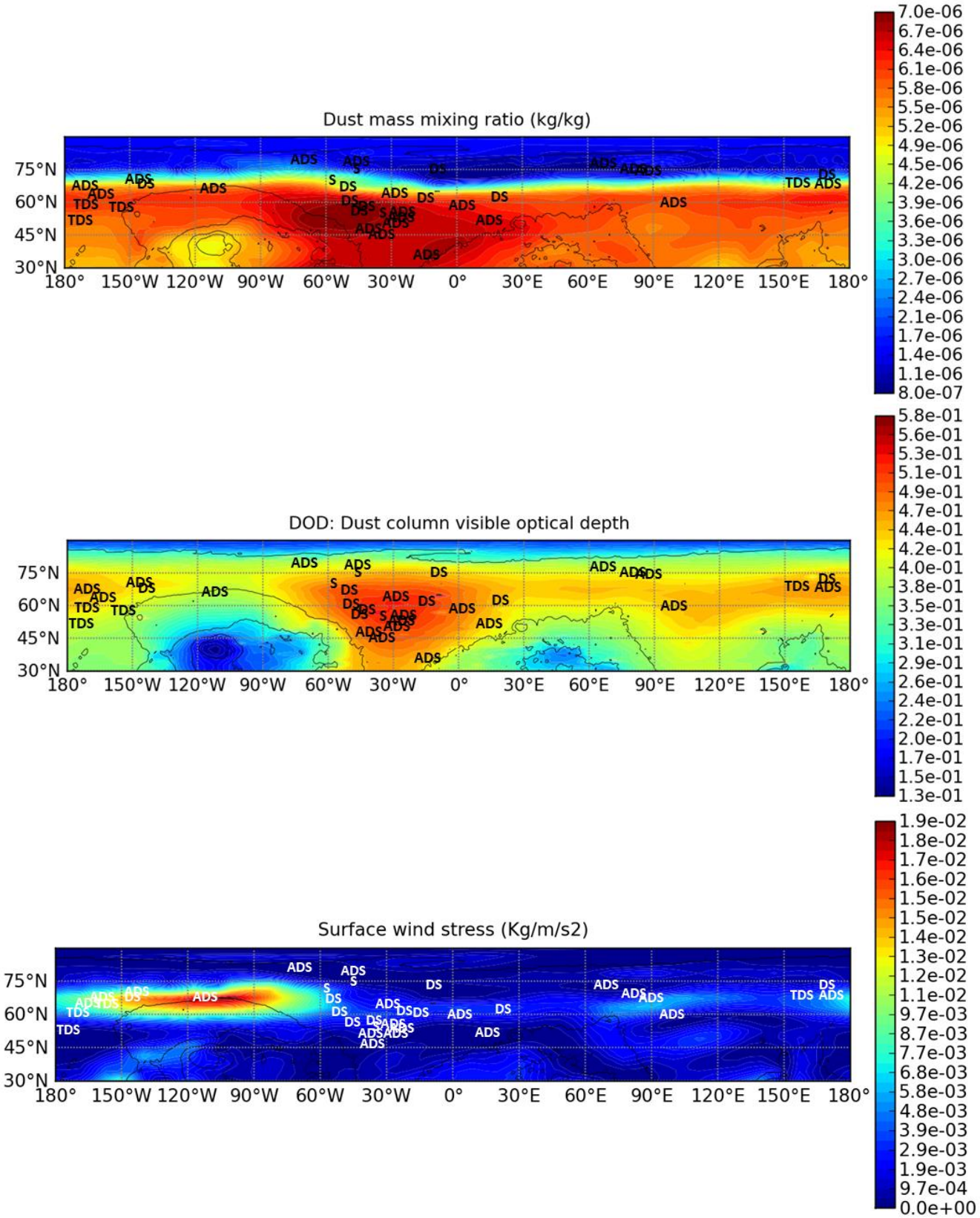


Figure 21. Dust mass mixing ratio (top), dust column visible optical depth (middle) and surface wind stress (bottom) at Ls=45$^{o}$ and 10 m height [MCD].

## 5.4 TEXTURED DUST STORMS

Four of these structures were spotted during the studied period and all of them took place near Ls=30º. The area, the speed (whenever possible) and the size of some of the characteristics of these dust storms have been measured. The location of the TDS (along with the spirals) is shown in Figure 22 and in Figure 23 an image of each TDS is shown. In Figure 23 can be seen the different kind of TDS that have been spotted, the first image shows a TDS that has three different fronts with cells in each one of them. The second shows a TDS that is found within a spiral, which has other features like water ice clouds, hazes and diffuse dust. The third and fourth images show a more compact kind of TDS.

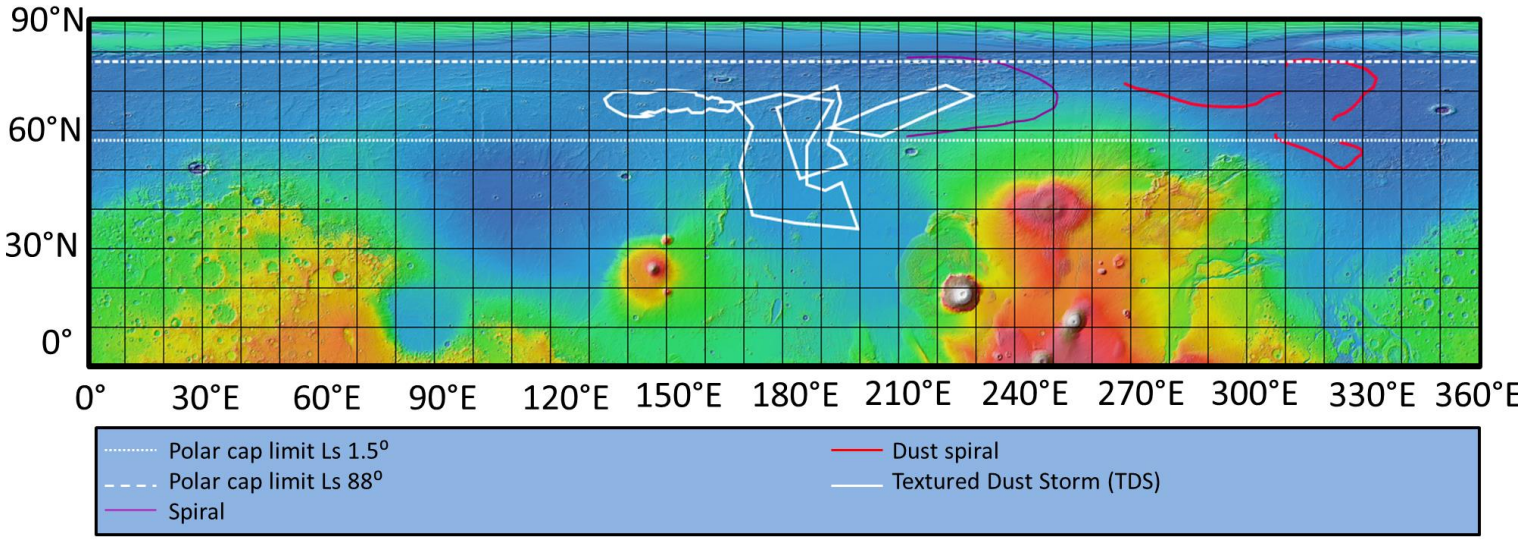


Figure 22. Location of the TDS and the spirals [JMARS].

All the TDS were spotted in the 140ºE - 240ºE longitude range, which places them over the Arcadia Planitia and one of them spreads into Amazonis Planitia. The northern limit of the TDS extends (except in one case) into the edge of the polar cap which might indicate that the gradient of temperature existent in that regions is involved in the development of this kind of structures, as occurred with the ADS.

The TDS have been classified using the criteria stated in [19 & 20] according to the area that the storm covers and the lifetime of the storm (in sols). At first, it was stablished in [19] that a regional dust storm has a long axis extending beyond 2000 km without encircling the planet. This was corrected later in [20], where a regional dust storm has an area $\geq 1.6 \cdot 10^6$ km$^2$ and staying active for more than 2 sols. Later, this last parameter was corrected in [21], changing it to 3 sols.

There is also another type of classification that can be made regarding the TDS [22]. It considers the textures of the visible cells within the storms stablishing three types: pebbled, plume-like and puffy.

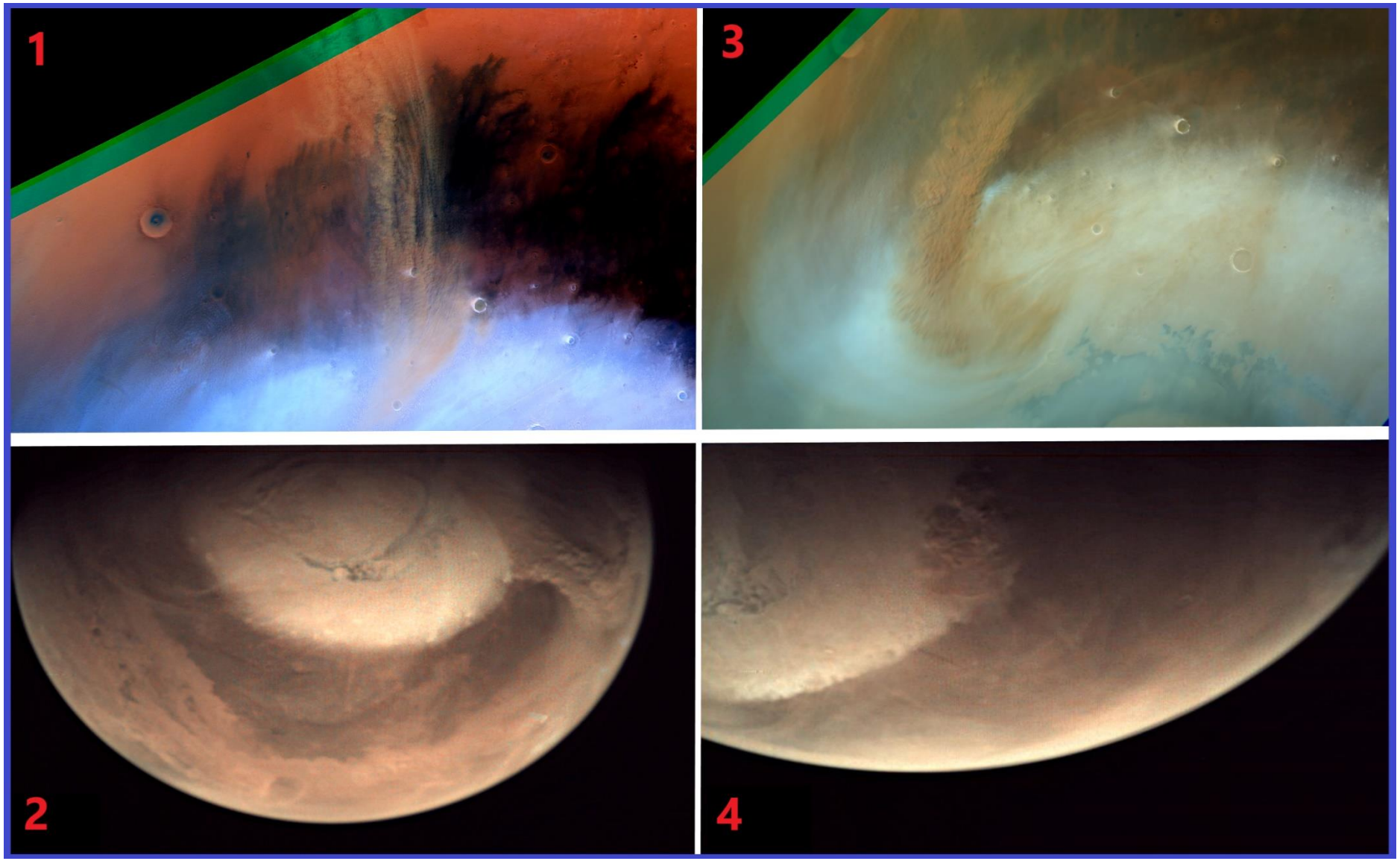


Figure 23. The four TDS that have been spotted [VMC & HRSC].

### 5.4.1 Textured Dust Storm May 22nd

The first TDS was captured by HRSC in May 22nd (Ls=28.6º) and it is shown in Figure 24 where its area has been marked in red. The whole storm is not visible, but the most important part of it can be analysed, specially the three visible fronts (numbered in the image), whose size and cells has been measured. An attempt of measuring the speed of this storm could not be made because it was only visible in one image, it was tried to find this structure in VMC's images but it was not possible.

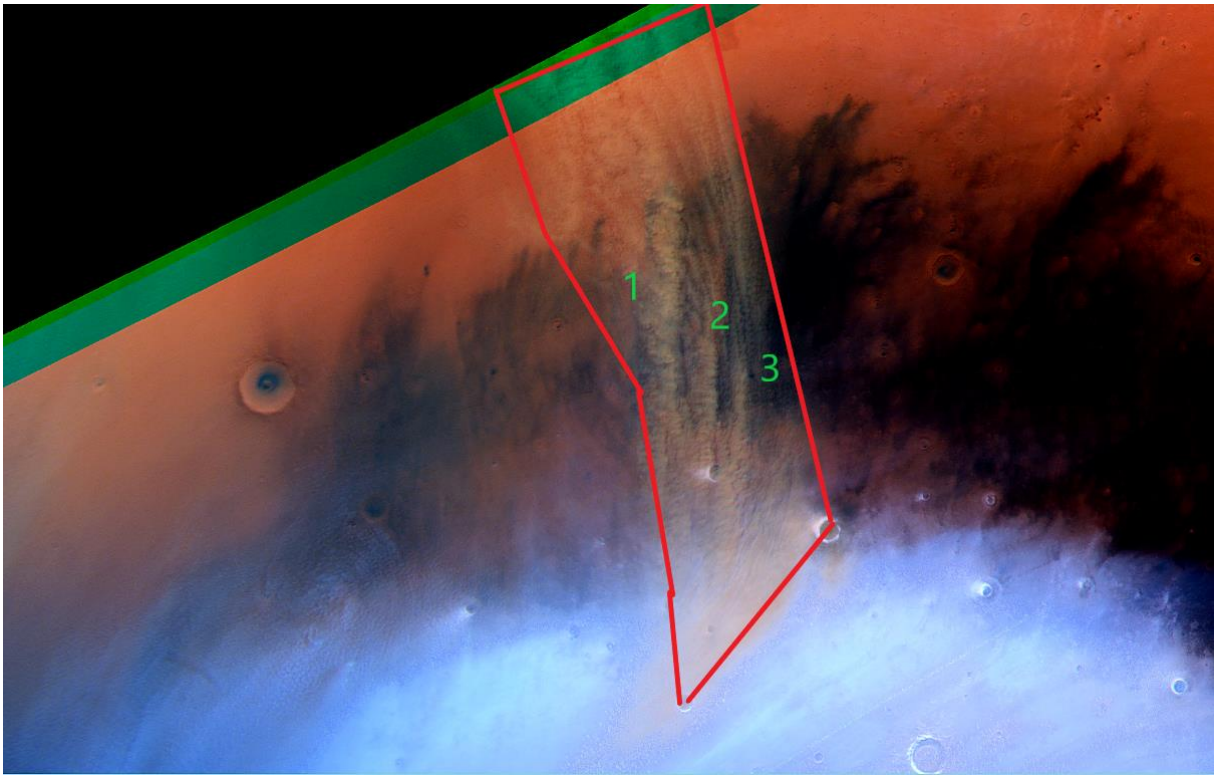


Figure 24. Area of the TDS spotted in May 22nd (Ls=28.6º) [HRSC].

According to its area, which is $4.3 \cdot 10^5$ km$^2$, this is a local storm. Regarding the other type of classification [22], this is a plume-like dust storm because it is composed by various elongated plumes (or fronts).

The measurements of the fronts and the cells are in Table 8 and 9, the fronts are numbered in Figure 24 and the cells are numbered in Figure 25.

| ***Table 8*** | | | |
|---|---|---|---|
| ***Front*** | ***Length (km)*** | ***Width (km)*** | ***Separation*** |
| 1 | 950.4 | 84.9 | 39.3 km (between 1 and 2) |
| 2 | 656.1 | 57.9 | 35.2 km (between 2 and 3) |
| 3 | 496.8 | 24.8 | - |

| *Table 9* | | | | |
|---|---|---|---|---|
| ***Cell*** | ***Front*** | ***Length (km)*** | ***Width (km)*** | ***Area ($km^2$)*** |
| 1 | 1 | 63.8 | 21.5 | 1077.9 |
| 2 | 1 | 62.1 | 20.7 | 1009.6 |
| 3 | 1 | 31.7 | 16.9 | 422.2 |
| 4 | 1 | 64.8 | 16.9 | 863.8 |
| 5 | 2 | 47.2 | 21.5 | 797.9 |
| 6 | 2 | 45.5 | 23.2 | 829.2 |
| 7 | 2 | 47.6 | 19.1 | 712.1 |
| 8 | 3 | 28.9 | 12.4 | 282.7 |
| 9 | 3 | 22.8 | 16.6 | 296.2 |
| 10 | 3 | 32.5 | 20.7 | 528.4 |

It is clear that the length of the cells is constrained by the width of the front. Therefore, the biggest cells are placed in the first front of the storm. The length to width ratio (l/w) changes in every front, with a l/w ~3 for the first front, l/w ~2 for the second front and l/w ~1.5 for the third front.


Figure 25. Measured cells for the TDS May 22$^{th}$ (Ls=28.6$^{o}$) [HRSC].

### 5.4.2 Textured Dust Storm May 26th

The second TDS was captured by HRSC in May 26th (Ls=30.4º). This is a very particular structure because it combines different types of phenomena, involving clouds, hazes, scattered dust, and a spiral. All this is marked in Figure 26 with a colour code that is described in the image itself.

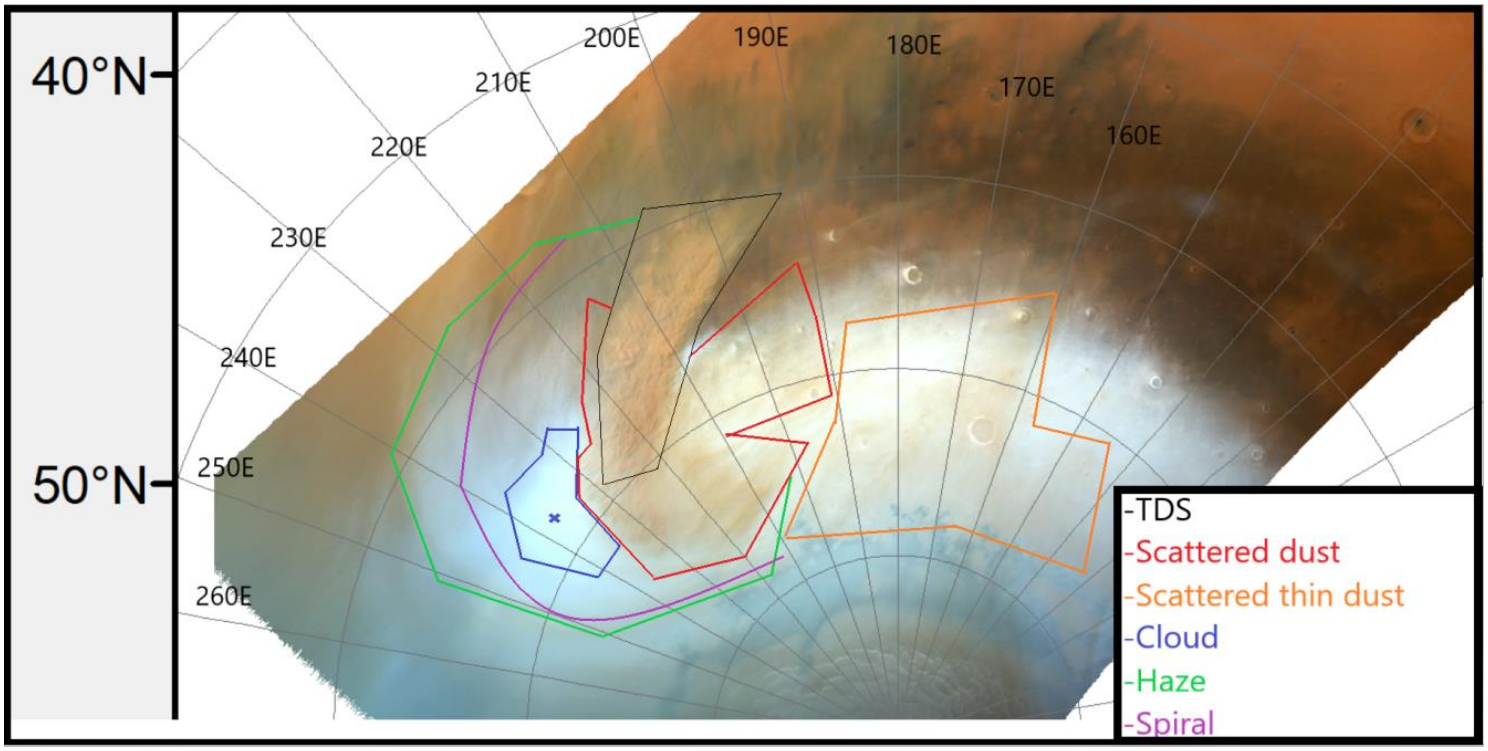


Figure 26. TDS and other structures spotted in May 26th (Ls=30.4º) [HRSC].

As with the TDS seen in May 22, it was not possible to determine its speed because there was only one image of it and no image of it was found in VMC's gallery.

This TDS has an area of $2.57 \cdot 10^5$ km$^2$ so it is also a local storm and based on the shape of the structure it can be considered a pebbled-type TDS. It could be argued that this is also a plume-like TDS but as no consistent pattern in the cells is identified the pebbled-type option seems more adequate.

In this case, the TDS has a unique front so the cells do not have the same size constraints as the previous one, consequently a bigger number of cells (Figure 27) have been measured in order to have a better understanding of the them.

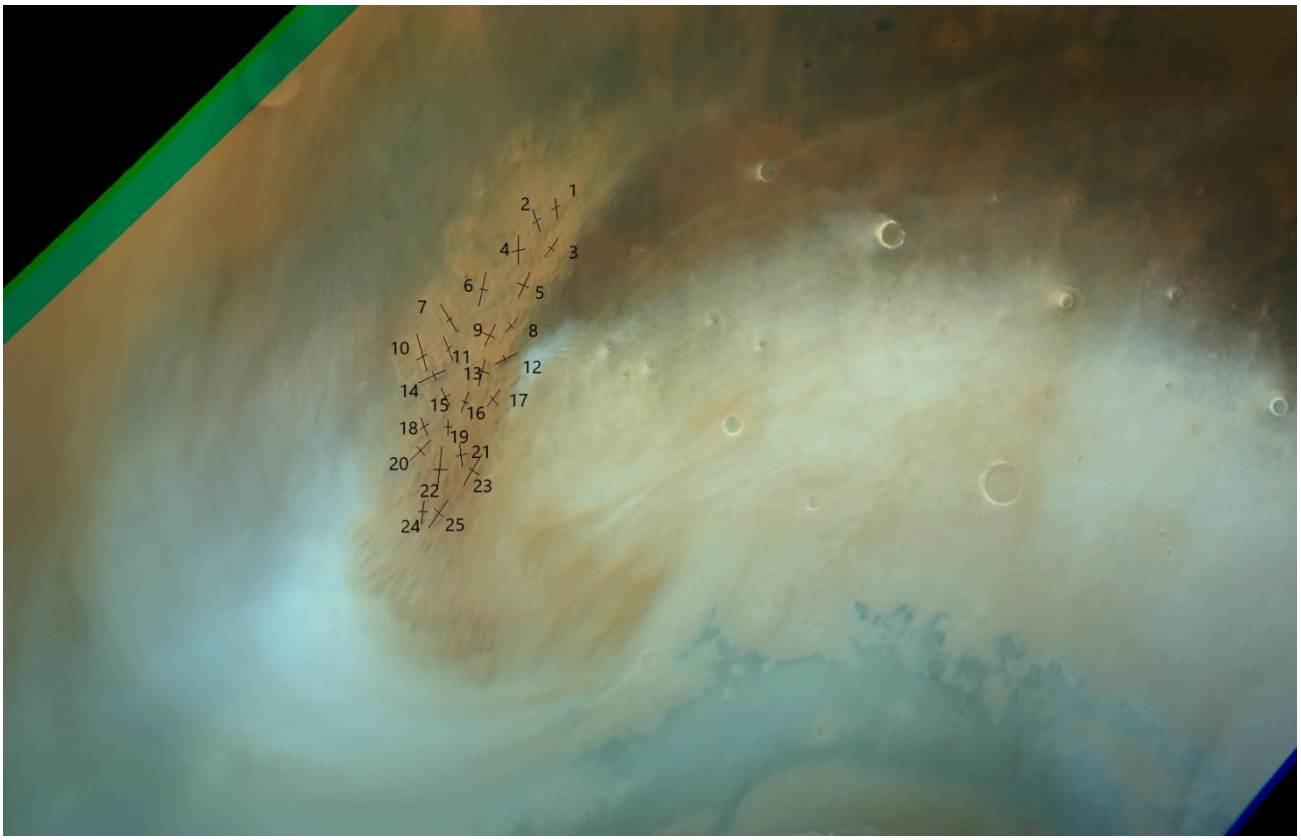


Figure 27. Measured cells [HRSC].

Not only the size of the cells has been measured, but also the distance between them. This has been done by measuring the distance that separates one cell with the two cells that are closer to it. The cells of this storm are similar in size to those of the storm analysed in the previous section. The mean value and standard deviation of their length, width, area and distance has been calculated and is given in Table 10. The l/w ratio of the cells is ~ 2.5 and the dimensions of each cell are shown in Table 11.

| ***Table 10*** | | |
|---|---|---|
| ***Parameter*** | ***Mean value (km)*** | ***Standard deviation (km)*** |
| Length (km) | 51.7 | 12.8 |
| Width (km) | 20.8 | 4.8 |
| Area ($km^2$) | 863.1 | 353.4 |
| Distance (km) | 56.1 | 15.7 |

| *Table 11* | | | |
|---|---|---|---|
| ***Cell*** | ***Length (km)*** | ***Width (km)*** | ***Area ($km^2$)*** |
| 1 | 38.9 | 19.3 | 591.5 |
| 2 | 47.6 | 19.1 | 711.3 |
| 3 | 43.7 | 15.8 | 541.2 |
| 4 | 59.5 | 26.1 | 1215.6 |
| 5 | 51.9 | 24.7 | 1006.1 |
| 6 | 67.1 | 14.1 | 744.1 |
| 7 | 62.7 | 14.9 | 732.9 |
| 8 | 36.9 | 15.8 | 456.5 |
| 9 | 47.9 | 27.9 | 1051.3 |
| 10 | 73.9 | 25.3 | 1467.3 |
| 11 | 47.9 | 15.8 | 592.8 |
| 12 | 47.9 | 15.5 | 581.6 |
| 13 | 54.9 | 24.9 | 1076.6 |
| 14 | 55.3 | 19.3 | 839.8 |
| 15 | 39.3 | 22.3 | 687.7 |
| 16 | 42.8 | 13.2 | 445.1 |
| 17 | 41.3 | 26.3 | 854.5 |
| 18 | 36.7 | 22.8 | 656.3 |
| 19 | 31.2 | 14.9 | 364.7 |
| 20 | 55.8 | 24.2 | 1061.5 |
| 21 | 46.5 | 22.7 | 831.7 |
| 22 | 80.7 | 28.3 | 1791.7 |
| 23 | 71.4 | 24.7 | 1383.8 |
| 24 | 46.5 | 17.8 | 652.3 |
| 25 | 65.1 | 24.2 | 1239.9 |

### 5.4.3 Textured Dust Storm May 29th

The third TDS was spotted in May 29th (Ls=32º) by VMC. This last aspect allowed to measure its speed as there were various images of the storm available. Five points of the storm were selected (Figure 28), each of them with a different latitude in order to evaluate how the speed changes with that parameter.

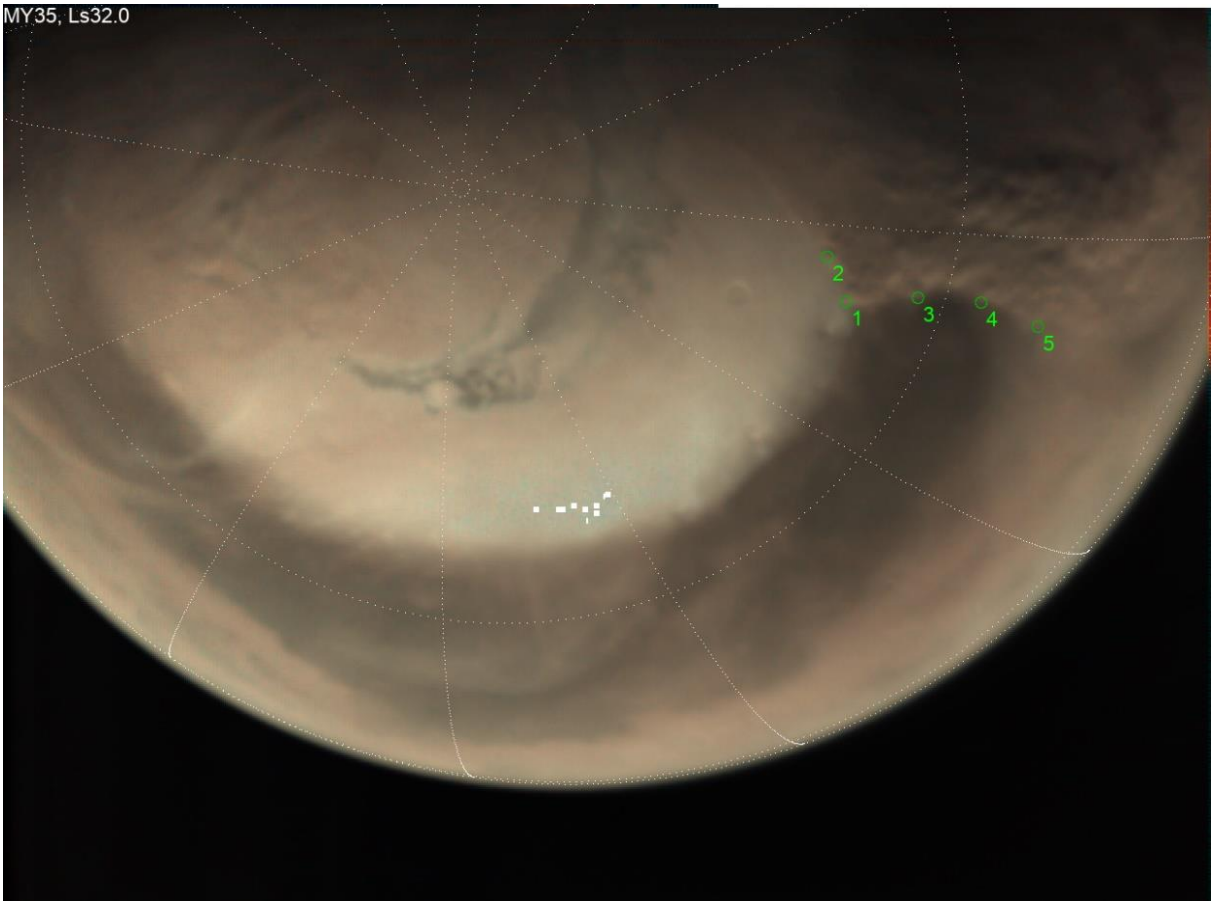


Figure 28. Points selected to measure the speed of the TDS May 29th (Ls=32º) [VMC].

The results of these measurements are shown in Table 12. It can be seen that the edge of the storm where the selected points are, did not move homogeneously at the same speed because the winds driving the storm change with latitude. This causes a distortion of the storm's edge with time. This storm drifted with a mean speed of 28 $ms^{-1}$.

| ***Table 12*** | | | |
|---|---|---|---|
| ***Point*** | ***Latitude*** | ***Longitude*** | ***Mean speed ($ms^{-1}$)*** |
| 1 | 66º N | 168º E | 32 |
| 2 | 68º N | 174º E | 42 |
| 3 | 62º N | 171º N | 28 |
| 4 | 57º N | 172º N | 22 |
| 5 | 52º N | 170º N | 17 |

With respect of the classification of the storm, its area was measured using the same technique applied in the other cases resulting in a value of $1.36 \cdot 10^6$ km$^2$ so it is a local storm. According to the shape of the cells (Figure 28) it has been considered that this storm is pebbled-type.

In this occasion a classification of the cells has also been done as a function of their size and area (Figure 29):

- Big: cells with an area > 8000 km$^2$.
- Medium: cells with an area between 5000-8000 km$^2$.
- Small: cells with an area < 5000 km$^2$.

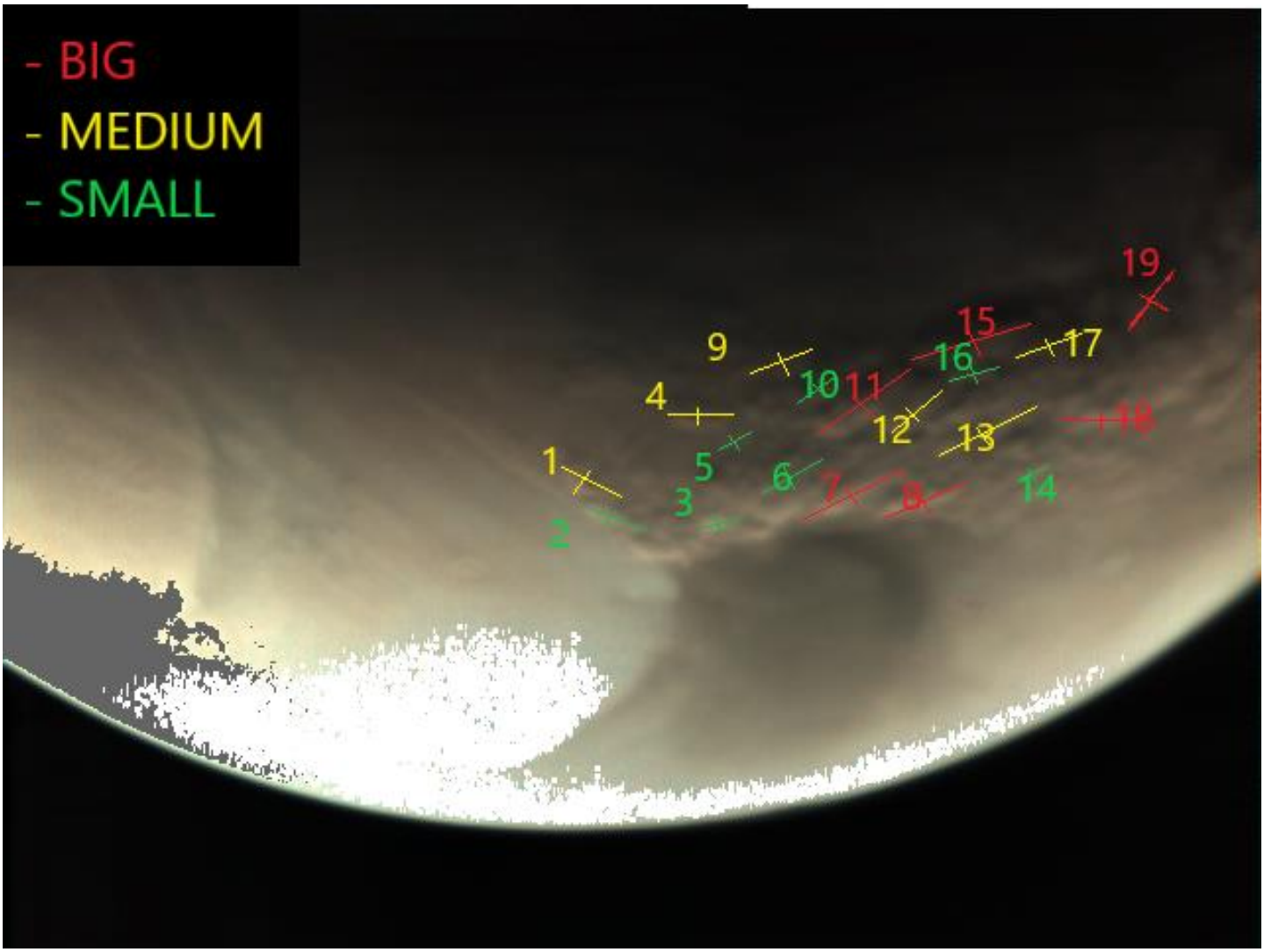


Figure 29. Cells in TDS May 29$^{th}$ (Ls=32$^o$) [VMC].

The bigger cells form only in the mid-lower latitudes where the storm developed. In Tables 13 the size of the cells is presented, and the mean values of the dimensions and the distances between cells have also been calculated (Table 14). From the calculations it can be said that this storm's cells present a l/w ratio of ~ 2.5.

| ***Table 13*** | | | |
|---|---|---|---|
| ***Cell*** | ***Length (km)*** | ***Width (km)*** | ***Area ($km^2$)*** |
| 1 | 123.3 | 65.2 | 6314.6 |
| 2 | 97.8 | 46.6 | 3577.1 |
| 3 | 66.2 | 54.8 | 2846.6 |
| 4 | 130.4 | 71.3 | 7301.1 |
| 5 | 89.5 | 51.2 | 3599.4 |
| 6 | 148.9 | 40.8 | 4766.9 |
| 7 | 191.6 | 63.8 | 9607.1 |
| 8 | 171.3 | 60.7 | 8165.9 |
| 9 | 137.5 | 61.8 | 6678.9 |
| 10 | 107.7 | 56.5 | 4778.9 |
| 11 | 198.2 | 79.4 | 12359.8 |
| 12 | 117.9 | 67.4 | 6235.9 |
| 13 | 184.9 | 39.7 | 5769.7 |
| 14 | 92.7 | 41.5 | 3019.4 |
| 15 | 241.6 | 62.8 | 11914.9 |
| 16 | 102.2 | 51.2 | 4109.6 |
| 17 | 140.9 | 61.1 | 6755.1 |
| 18 | 193.8 | 80.7 | 12291.8 |
| 19 | 129.2 | 100.3 | 10181.1 |

| ***Table 14*** | | |
|---|---|---|
| ***Parameter*** | ***Mean value*** | ***Standard deviation*** |
| Length (km) | 140.3 | 45.8 |
| Width (km) | 60.9 | 15.2 |
| Area ($km^2$) | 7009.1 | 3146.2 |
| Distance (km) | 179.6 | 62.8 |

### 5.4.4 Textured Dust Storm June 3rd

The last TDS was also captured by VMC, so it was possible to measure its speed. This TDS, captured in June 3rd (Ls=34º) presents a feature that makes it different to all the others. As it can be seen in Figure 30 this storm has a very small meridional development presenting an almost ellipse-like shape. In that figure the points that have been used to measure the speed are marked.

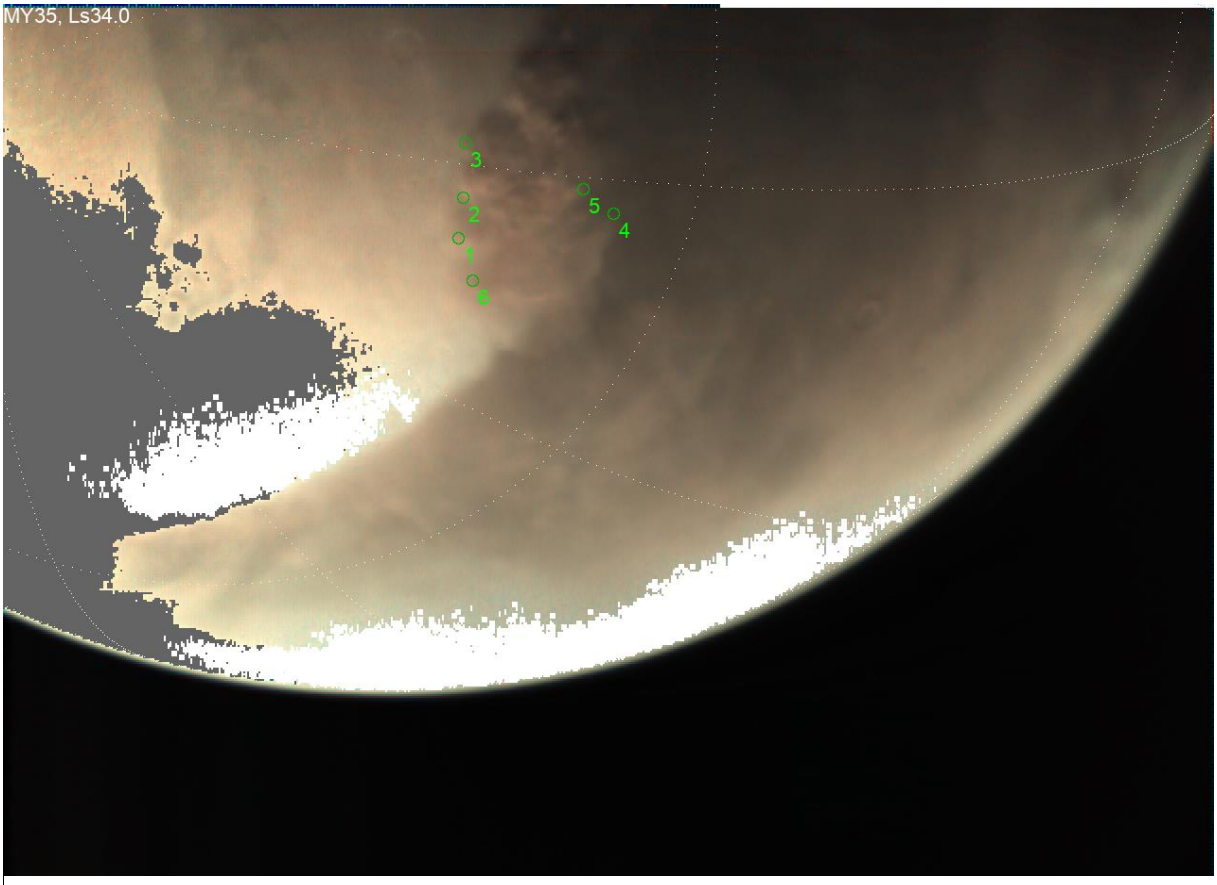


Figure 30. TDS spotted in June 3 (Ls=34º) [VMC].

The results of the speed's measurement are shown in Table 15. The procedure that has been followed is the same which was followed with the third TDS. This storm does not show the same tendency in terms of speed (lower speed in lower latitudes) as the previous storm did.

| *Table 15* | | | |
|---|---|---|---|
| ***Point*** | ***Latitude*** | ***Longitude*** | ***Mean speed ($ms^{-1}$)*** |
| 1 | 70º N | 139º E | 42 |
| 2 | 70º N | 145º E | 45 |
| 3 | 70º N | 152º E | 40 |
| 4 | 63º N | 146º E | 41 |
| 5 | 65º N | 149º E | 25 |
| 6 | 68º N | 134º E | 33 |

Another special circumstance of this TDS is that it was fully spotted in images that were taken in three different days. Therefore, the evolution of this TDS its area can be tracked (Table 16). The storm has an area with a mean value of $1.83 \cdot 10^5$ km$^2$ and therefore it is classified as a local storm.

| *Table 16* | |
|---|---|
| ***Day*** | ***Area (km$^2$)*** |
| ***June 2$^{nd}$ (22:55 h)*** | $\mathbf{1.805 \cdot 10^5}$ |
| ***June 3$^{rd}$ (00:23 h)*** | $\mathbf{2.11 \cdot 10^5}$ |
| ***June 5$^{th}$ (01:15 h)*** | $\mathbf{1.6 \cdot 10^5}$ |

As it was done with the other TDS based on the cells' shape, from the images of June 3$^{rd}$ (Figure 30) the storm would fit in the pebbled-type storm but the images from June 5$^{th}$ (Figure 31) suggest that it could be a puffy-type storm because the cells have a cotton-like inflated structure. However, this might be due to the final evolution of the TDS as it might be in its final stage, aspect that is suggest by the reduction of the area.

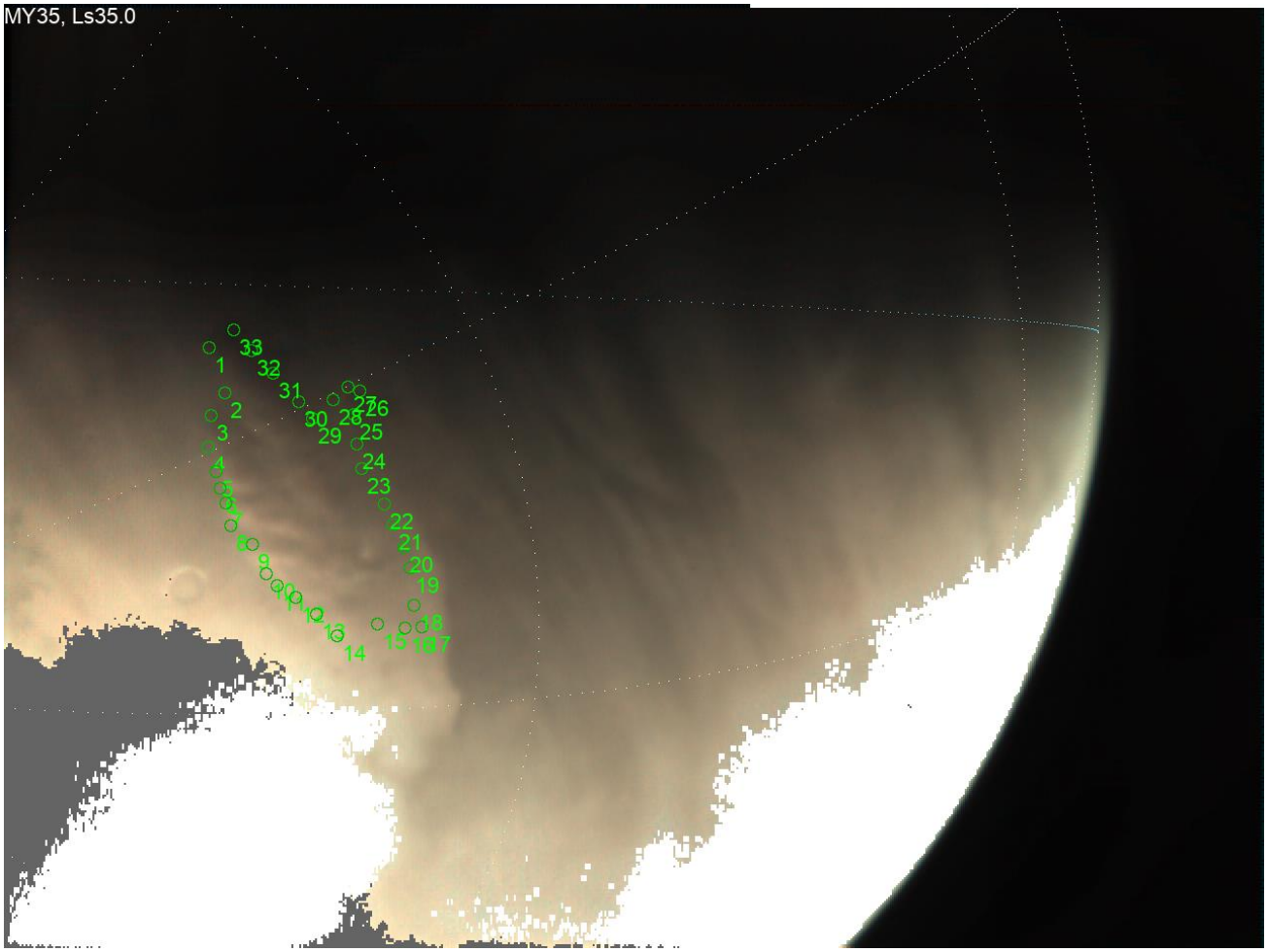


Figure 31. Fourth TDS in June 5th [VMC].

In the analysis of the cells (Figure 32) a classification of them has also been made with the following considerations:

- Big: cells with an area > 4000 $km^2$.
- Medium: cells with an area between 2000-4000 $km^2$.
- Small: cells with an area < 2000 $km^2$.

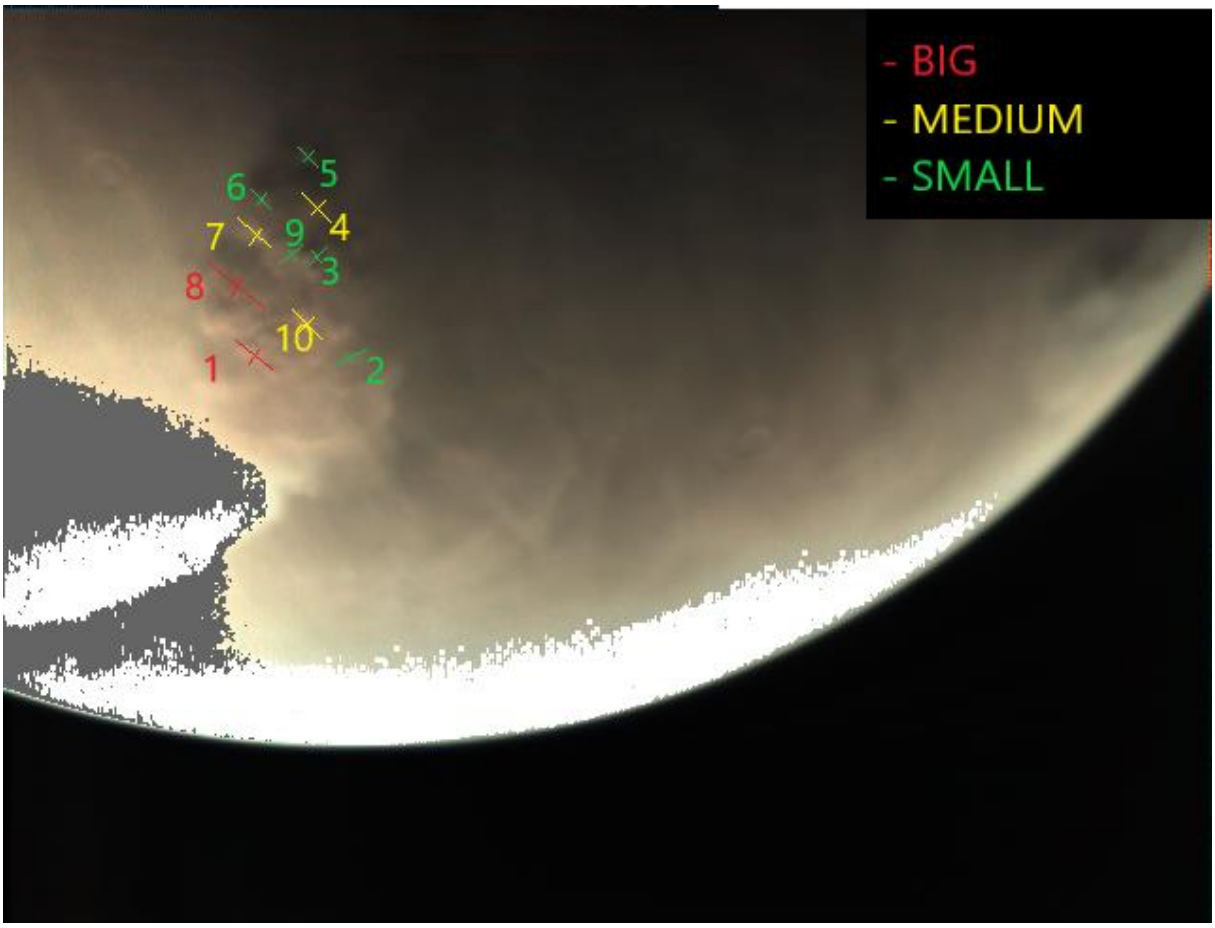


Figure 32. Cell type identification according to their area, June 3rd (Ls=34º) [VMC].

Most of the cells are rather small compared to the cells of previous studied TDS, this is a consequence of the size of the storm. Another detail that can be seen in Figure 32 is that almost all of them are located in the eastern part of the storm. In this case the l/w ratio is ~ 1.6 and the results are given in Table 17 and 18.

| ***Table 17*** | | |
|---|---|---|
| ***Parameter*** | ***Mean value*** | ***Standard deviation*** |
| Length (km) | 70.7 | 17.7 |
| Width (km) | 42.3 | 8.6 |
| Area ($km^2$) | 2408.5 | 1041.9 |
| Distance (km) | 119.1 | 31.9 |

| *Table 18* | | | |
|---|---|---|---|
| ***Cell*** | ***Length (km)*** | ***Width (km)*** | ***Area ($km^2$)*** |
| 1 | 102.3 | 52.5 | 4215.3 |
| 2 | 54.8 | 41.2 | 1773.5 |
| 3 | 56.3 | 31.8 | 1406.4 |
| 4 | 68.3 | 46.8 | 2512.7 |
| 5 | 54.3 | 41.7 | 1780.4 |
| 6 | 54.9 | 41.4 | 1785.9 |
| 7 | 63.2 | 41.5 | 2055.9 |
| 8 | 94.6 | 58.9 | 4383.2 |
| 9 | 73.1 | 33.1 | 1893.7 |
| 10 | 85.4 | 33.9 | 2277.8 |

### 5.4.5 Analysis and comparison of the TDS

To make a quick comparison of the different TDS, in Table 19 a summary of the main properties of this kind of storm is presented.

***Table 19***

| ***TDS*** | ***Instrument*** | ***Area ($km^2$)*** | ***Type*** | | ***Mean speed ($ms^{-1}$)*** | ***Cells*** | | | |
|---|---|---|---|---|---|---|---|---|---|
| | | | ***Area*** | ***Shape*** | | ***Mean length (km)*** | ***Mean width (km)*** | ***Mean area ($km^2$)*** | ***~ l/w*** |
| May 22nd | HRSC | $4.3 \cdot 10^5$ | Local | Plume | - | 44.7 | 18.9 | 682.1 | 2.3 |
| May 26th | HRSC | $2.57 \cdot 10^5$ | Local | Pebbled | - | 51.7 | 20.8 | 863.1 | 2.5 |
| May 29th | VMC | $1.36 \cdot 10^6$ | Local | Pebbled | 28 | 140.3 | 60.9 | 7009.1 | 2.5 |
| June 3rd | VMC | $1.83 \cdot 10^5$ | Local | Pebbled | 37 | 70.7 | 42.3 | 2408.5 | 1.6 |

From that comparison it can be argued that the most common type of TDS in the north polar region during the spring is the local-pebbled storm, but the sample is too small to be certain of all aspects. The determination of the TDS' type (regarding the shape) is considered important because it gives clues about the atmospheric conditions, as each one of those types of TDS are tied to specific conditions [22].

- The pebbled-type suggests strong turbulence which is associated with strong wind shear.
- The puffy-type indicates vertical development and convection as these structures are similar to terrestrial cumulus.
- The plume-type suggests dust lifting by strong winds.

One aspect that is almost the same in all the observed TDS is the l/w ratio (~ 2.5) because the other dimensions (length and width) rely on the size of the storm. Therefore, the obtained ratio might be a constant in the TDS that developed in that period of time. The last aspect that needs to be compared is the data from MCD and the measurements that have been obtained. MCD does not predict TDS development but the data on wind speed and surface wind stress might give a clue of the regions that are prone to present this kind of phenomena.

The first parameter is the surface wind stress (Figure 33) predicted by MCD. There is only one zone with values over 0.01 Pa (limit which was mentioned before for uplifts) and occurs between 55°N - 70°N. This means that this particular zone is prone to trigger dust lifting events which might end up causing phenomena like the observed TDS, some of which are precisely placed in that range of latitudes.

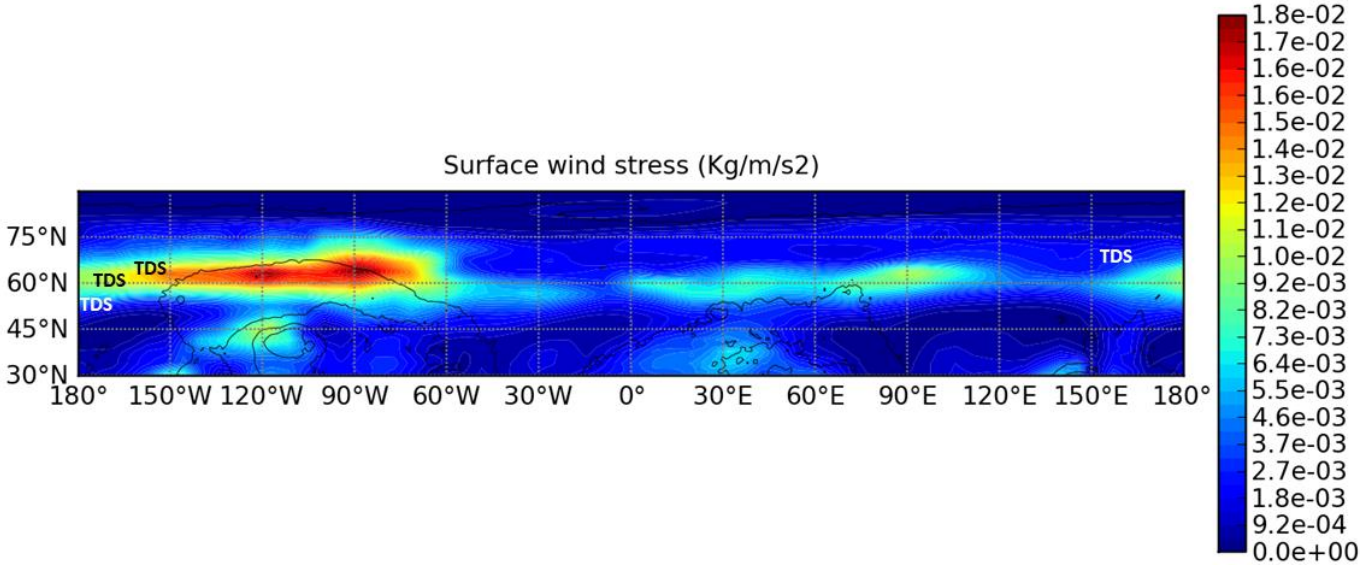


Figure 33. Surface wind stress Ls=30° at Z=10 m[MCD].

Another parameter that has been compared is the wind's values (Figure 34). Not only the horizontal wind has been studied but also the vertical component has been checked. This component might indicate the existence of zones with active vertical winds that end creating instabilities in the atmosphere.

The MCD height data that fits better with the measured speed is 10 km. It corresponds to a speed of ~ 25 $ms^{-1}$ for the TDS of May 29$^{th}$ (28 $ms^{-1}$ were measured) and a speed of ~ 40 $ms^{-1}$ for the TDS of June 3$^{rd}$. Regarding the vertical wind, MCD predicts null values (Figure 34 bottom) for the zones were both TDS were spotted so nothing can be concluded in regard to this aspect.

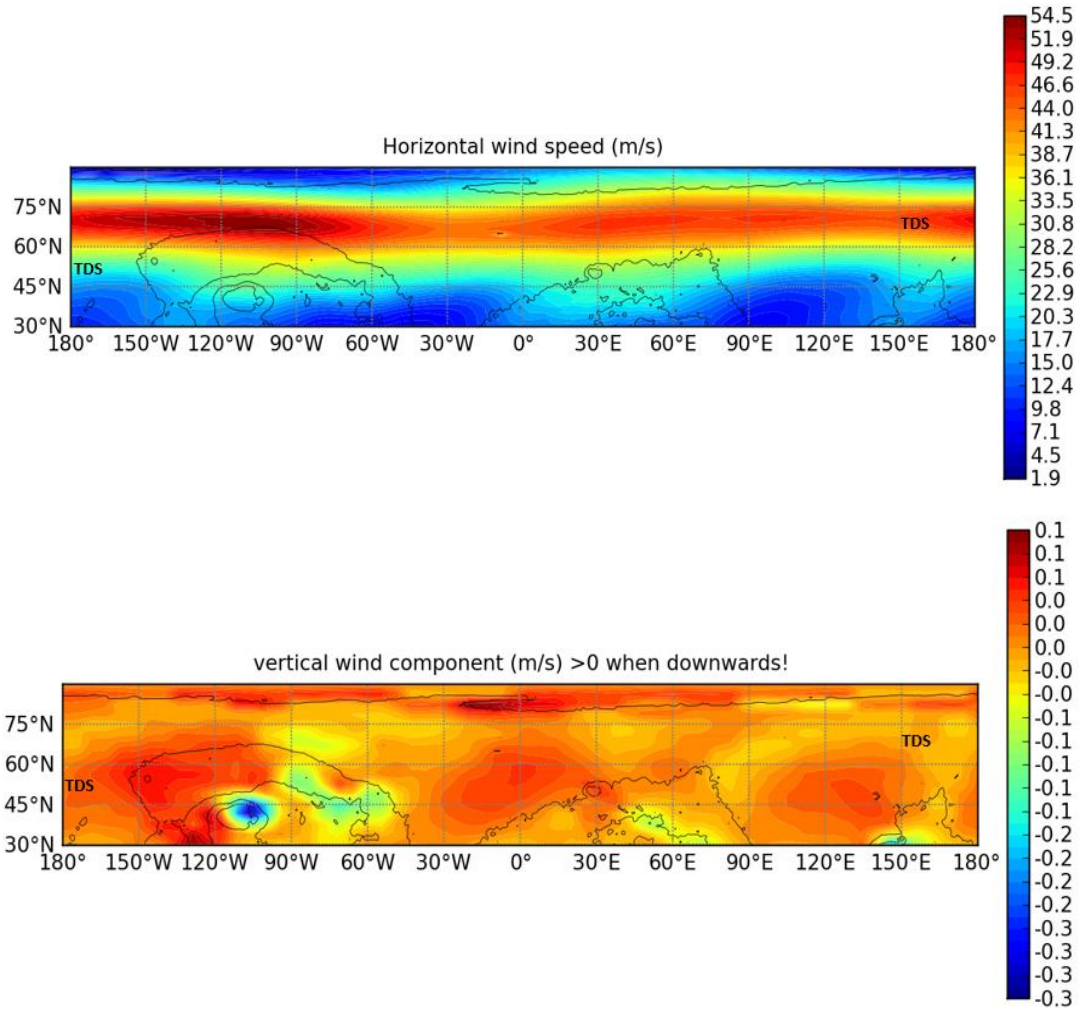


Figure 34. Horizontal wind speed (top) and vertical wind component (bottom) in Ls=30$^{o}$ and 10 km height [MCD].

## 5.5 SPIRAL FORMATIONS

Three spirals are reported in this project (Figure 22). Two of them are composed mostly by dust (one of them is a double spiral) and the other one is composed by water ice. All three were located near the edge of the polar cap and measurements of their sizes and speed has been performed.

### 5.5.1 Spiral May 26th

The first spiral (Figure 35 top) was captured by HRSC in May 26$^{th}$ (Ls=30$^{o}$) along with other structures that have already been studied. Its longitude has been measured and also its speed as this feature was identified also in an image taken by VMC (Figure 35 bottom) hours later. The TDS has already disappeared but the location and longitude of the structure suggests that is the same.

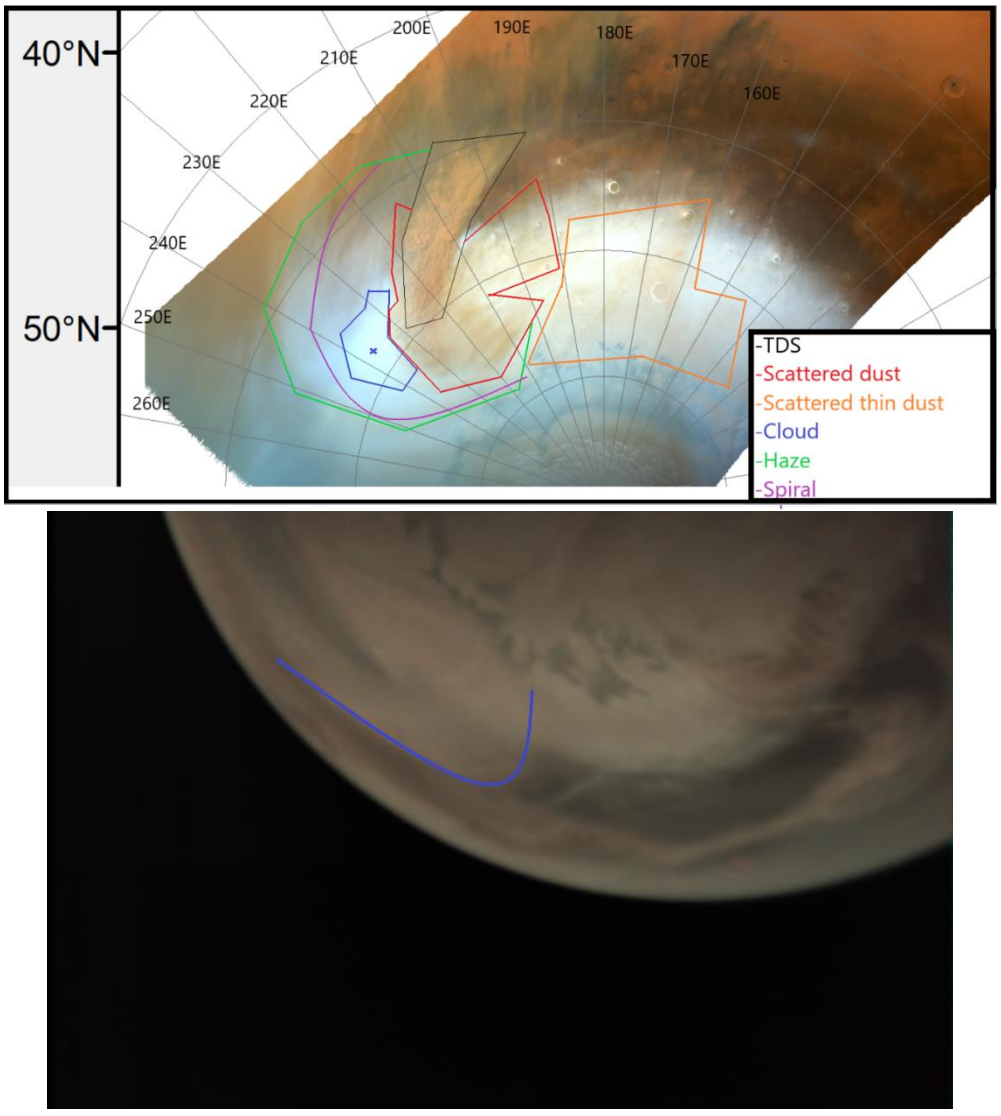


Figure 35. Spiral captured by HRSC (top, May 26$^{th}$) and the same spiral captured by VMC (bottom, May 27$^{th}$) hours later.

The longitude measured in HRSC's image is 2080 km and in the VMC's image is 1955 km, with that difference, which is rather small (~ 5%) and a latitude of the structure's centre almost identical (67°N in HRSC and 64°N in VMC) it has been decided that both structures are the same. In VMC's image the TDS has disappeared and the spiral is now composed by a mix of dust and water ice, meanwhile in HRSC's image the structure was exclusively formed by water ice.

There was another possible interpretation that involves the feature that can be seen in the bottom-right part of Figure 35. This feature is a second spiral and it could be argued that it is the same spiral seen in May 26th by HRSC. This has been discarded for the following reasons.

- The second spiral is located at 55° N which is far more southwards than the first one. If it is the same it would imply a large displacement to the south, which seems highly unlikely as is has not been seen in other structures in such a short period of time (less than 24 hours)
- The second spiral is almost exclusively composed by dust, while, the first spiral was composed by water ice

The centre of this spiral is located at 67°N - 240°E and its meridional size was 887 km.

Once it is settled that the spiral is present in two different images, its speed can be measured tracking the motion of its centre between two observations and a value of 16 $ms^{-1}$ has been obtained.

### 5.5.2 Spiral May 27th

The second spiral has already been shown in Figure 35 but a better look of it is presented in Figure 36. It was captured by VMC in May 27th (Ls=31°) hours later than the first spiral. This spiral is almost exclusively composed by dust and its shape suggests that it is in either its early or its final stages because it shows less clear structure almost like it is already broken or in a decay-like phase.

The centre of this spiral is located at 55°N - 346°E, it has a length of 1146 km and a meridional size of 719. As before, after tracking its displacement a horizontal velocity of 42 $ms^{-1}$ is obtained.

In Figure 36 another structure can be seen, which could even be a TDS but the image is not good enough to classified it as that. Besides, an attempt to find a better look of it to analyse the structure was made but there were no good results.

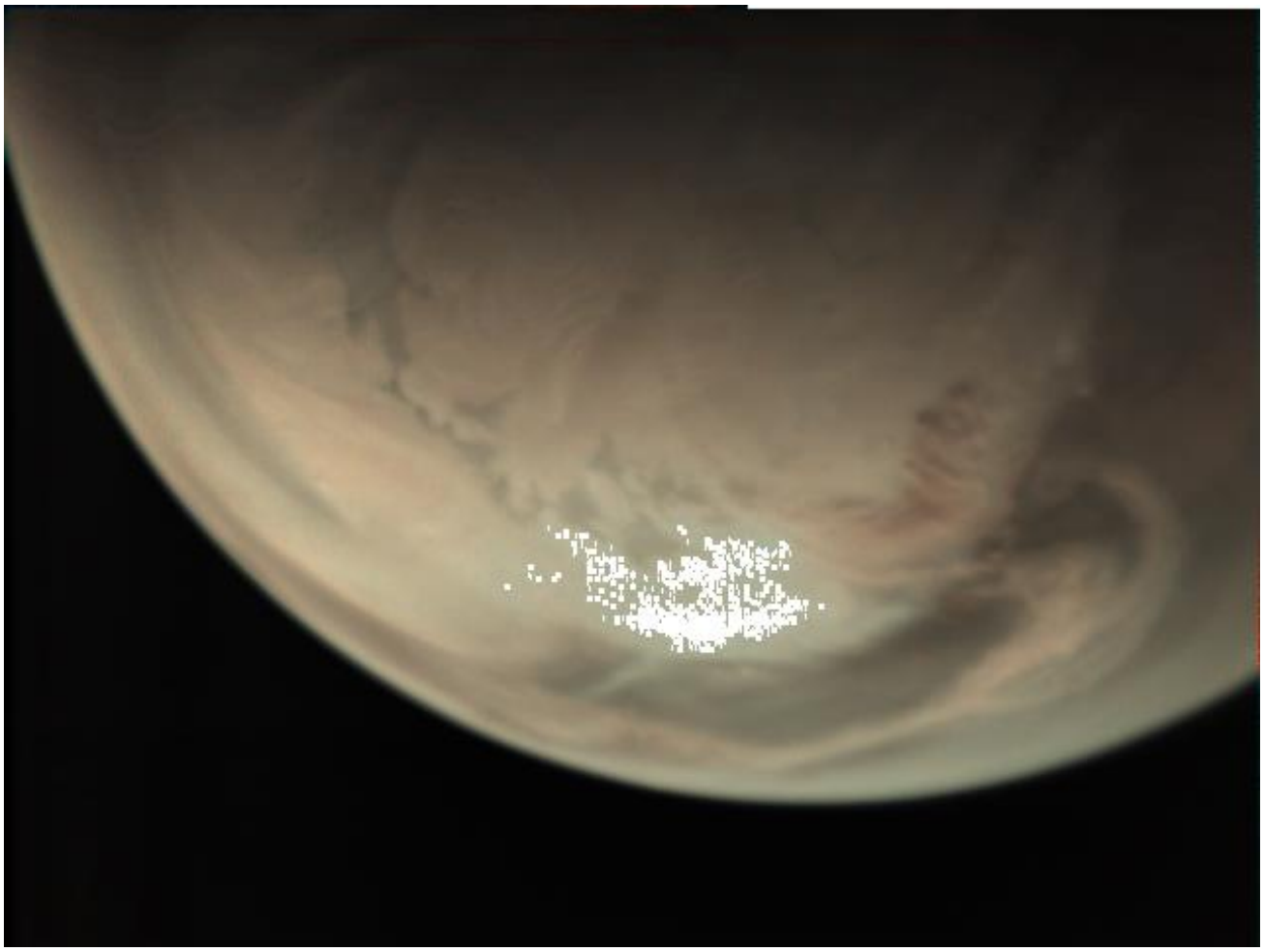

Figure 36. Second spiral May 27th (Ls=31º) [VMC].

### 5.5.3 Spiral October 1st

The last event was the most complex of the three reported spirals, because it is a double spiral as shown in Figure 37 (top). It was spotted in October 1st (Ls=88º) and in the following days. An example of the structures seen days later is shown in Figure 37 (bottom). The presence of the double spiral in various images allowed to measure its speed obtaining a value of 41 $ms^{-1}$.

Both spirals are mostly composed by dust but the presence of water ice in the form of hazes cannot be discarded. Table 20 gives the measured properties of this spiral

| ***Table 20*** | | | |
|---|---|---|---|
| ***Structure*** | ***Location (centre)*** | ***Length*** | ***Meridional size (km)*** |
| Spiral 1 | 72ºN 148ºE | 998 | 353 |
| Spiral 2 | 69ºN 183ºE | 1260 | 534 |

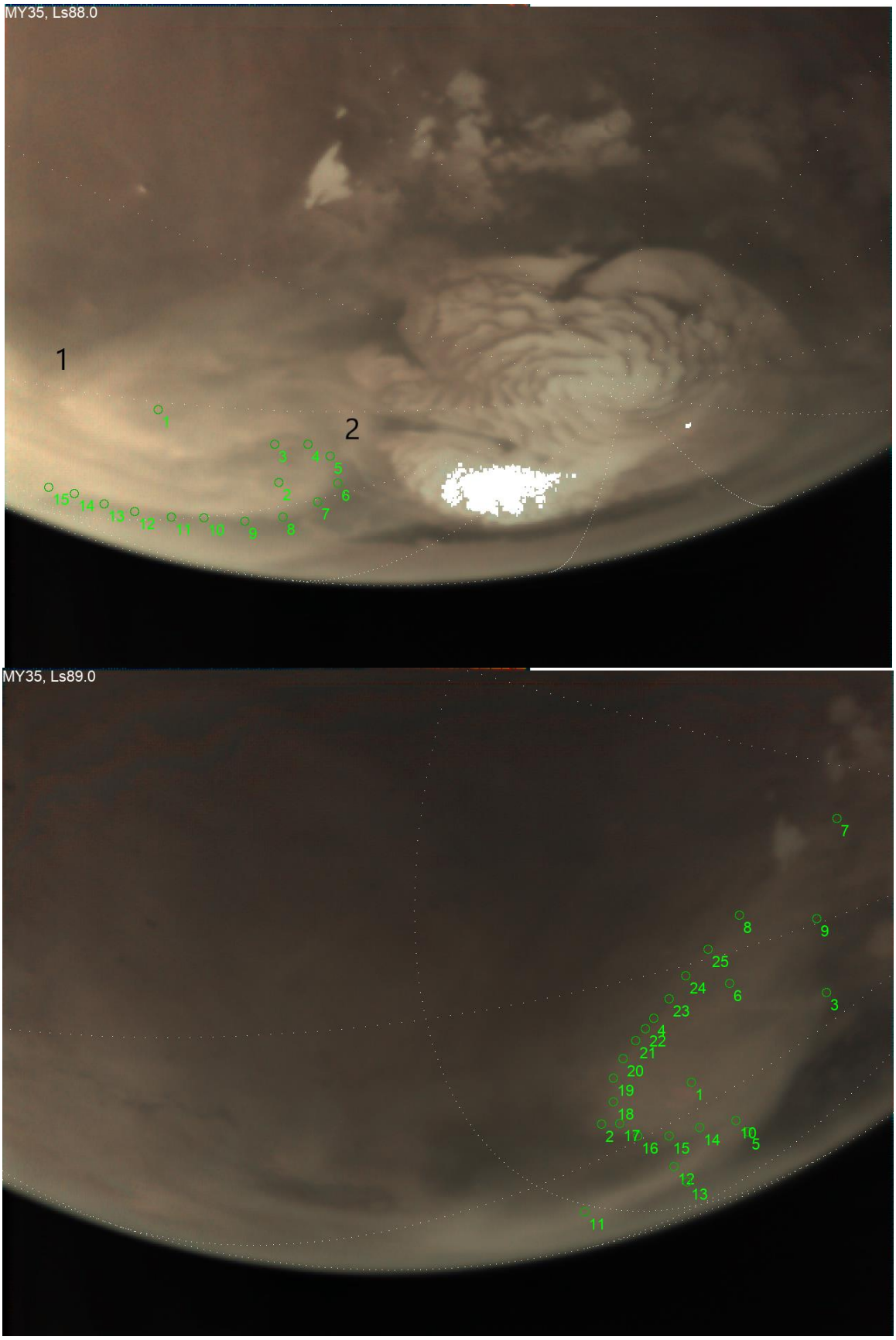


Figure 37. Double spiral (top, October 1st Ls=88º) and one of the two spirals developed three days later (bottom, October 4th Ls=89º) [VMC].

Table 21 summarizes the results of the measurements of the spiral systems. In the speed column the movement direction of each feature is given.

**Table 21**

| Identification | Instrument | Observation date | LTST | Ls | Centre (Lat., Lon.) | Meridional size (km) | Length (km) | Speed ($ms^{-1}$) | Properties |
|---|---|---|---|---|---|---|---|---|---|
| S1 | HRSC & VMC | May 26th<br>May 27th | 15h<br>11h | 30 | 67N 240E | 887 | 2080 | 16 (EAST) | Spiral composed by water ice along with other structures (TDS, scattered dust, haze) |
| S2 | VMC | May 27th | 14h | 31 | 55N 346E | 719 | 1146 | 42 (SOUTHEAST) | Spiral composed by dust |
| S3 (double) | VMC | October 1st | 10h | 88 | 72N 148E | 353 | 998 | 41 (SOUTHEAST) | Double spiral (mostly dust) with a distance between centres of 2234 km |
| | VMC | October 4th | 11h | 89 | 69N 183E | 534 | 1260 | | |

### 5.5.4 Theoretical analysis of the spirals

The theoretical analysis of these spirals is based on what it was presented in the master's subject Planetary Atmospheres, in those lectures it was explained that because of the rapid rotation of Mars, the atmosphere outside the Equator, is under geostrophic balance [24]. In that subject, the different kinds of instabilities that an atmosphere can develop were also addressed and for this kind of structures the baroclinic instability in the more suitable at the time of explaining these phenomena. The baroclinic instability is characterized for the existence of vertical shear in the atmosphere, meanwhile the barotropic instability is characterized by its absence. Therefore, the vertical shear (dU/dz) is the first marker that has been study in these calculations.

Other markers that have been used to study these spirals are the meridional wind's gradient (dV/dz) and the meridional temperature's gradient (dT/dy). These three markers combined have served to identify the regions of interest.

The procedure followed during the study of each spiral is the following and MCD was used to obtain the data:

- First, a preliminary region of interest is selected. The latitude range stablished ($50^oN$ - $90^oN$) corresponds to the location of the spirals and also the three longitudes chosen, which corresponds with the centre of the spirals. The Ls and hour that have been selected corresponds to that of the observed spirals. The height range goes from the surface to 20 km.
- The selected variables are zonal wind, meridional wind and temperature.
- With the data downloaded from MCD the dU/dz, dV/dz and dT/dy are calculated.
- An evaluation of the results of dU/dz, dV/dz and dT/dy is made. The baroclinic instability is increased where those values are large, therefore the definitive region of interest is determined by that criteria.
- The region of interest will consist in an interval of latitudes (5 degrees) and one scale-height.

Once the region of interest is determined, the calculations of the different parameters related to the baroclinic instability can be done. The first parameter is the Richardson number and depending on the values of this number the type of dynamical instability can be evaluated. In this case the values of the Richardson number should be in the 1<Ri<1000 interval [24], which is the predefined interval for baroclinic instabilities.

The Richardson number has been assessed in the whole height interval and to calculate it first other parameters must be defined (5), like the vertical temperature's gradient (dT/dz), the static stability (S) and the Brunt-Väisälä frequency (N). They are given by:

$$\frac{dT}{dz} = \frac{T_i - T_j}{Z_i - Z_j} \qquad S(z) = \frac{dT}{dz} + \frac{g}{C_p} \qquad N(z) = \sqrt{\frac{g}{T} \cdot S} \qquad (5)$$

The Richardson number (6) is then calculated and is represented in Figure 38.

$$Ri(z) = \frac{N(z)^2}{\left(\frac{dU}{dz}\right)^2} \tag{6}$$

The horizontal scale expected for the baroclinic disturbance (with the wavelength $L_x$) depends on Rossby deformation radius ($L_D$). Since an interval of latitudes is studied there will be two values (maximum and minimum) for Rossby's radius and for the wavelength. Both are given in (7).

$$L_D = \frac{N \cdot H}{f} \qquad L_x = 4 - 6 \cdot L_D \tag{7}$$

The scale height (H) and the Brunt-Väisälä frequency (N) used in that equation are the mean values obtained for those variables for their height interval. A comparison between the theoretical values and the measurements will be done later in this section.

But before, the parameters that have been used to study the spirals, applying the values obtained in the measurements, are addressed. The first one is the pressure's gradient force (dP/dr) and this parameter has been used in previous works [23] to study similar events like in that case a double cyclone. This equation (8) assumes that the vortices are in gradient wind balance, that is to say, a situation in which the pressure's gradient force, the Coriolis' force and the centrifuge force are in balance.

$$\frac{V^2}{r} + fV = \left|\frac{1}{\rho}\frac{\partial P}{\partial r}\right| \tag{8}$$

In this equation the radius (r) is the measured length of the spiral divided by 2. The density ($\rho$) is the value at the selected height (Z) and V is the rotational velocity of the vortex. The values of the pressure's gradient will be assumed for the vortex taking as a reference the values of the meridional pressure's gradient (dP/dy) in the atmosphere.

The last parameter that has been calculated is the radial temperature's gradient (dT/dr) using the thermal wind approximation [24]. A typical value of dV/dz has been used with v=15 $ms^{-1}$ for the selected height (Z), the value of temperature (T) is also the value of T at Z and as there is an interval of latitudes, there will be a maximum and minimum of dT/dr.

$$\frac{\partial V}{\partial z} = -\frac{g}{f \cdot T}\frac{\partial T}{\partial r} \tag{9}$$

Once the calculations have been completed, the results have been gathered in Table 22. Another parameter (Rossby number, Ro) has been added to the calculations, if the condition Ro<1 is verified then the vortex can be considered in gradient wind's balance. The identification (Id.) of the spirals is the same used in the previous section (Table 21) with two values for some of the parameters in the case of S3 because it was a double spiral.

**Table 22**

| Id. | LTST | Ls | Latitude (ºN) | Longitude (ºE) | Z (km) | $L_x$ (km) | $L_D$ (km) | Ro | dP/dr (mbar/km) | dT/dr (K/km) | dP/dy (mbar/km) |
|---|---|---|---|---|---|---|---|---|---|---|---|
| S1 | 15h | 30º | 67-72 | 240 | 6 | 3349 – 3622 | 575 - 604 | 0.11 – 0.10 | $2.8\cdot10^{-4}$ / $3.1\cdot10^{-4}$ | $-1.3\cdot10^{-2}$ / $-1.3\cdot10^{-2}$ | $3.1\cdot10^{-4}$ |
| S2 | 14h | 30º | 63-68 | 346 | 4 | 3739 - 3701 | 623 – 617 | 0.55 – 0.53 | $1.4\cdot10^{-3}$ / $1.5\cdot10^{-3}$ | $-1.1\cdot10^{-2}$ / $-1.3\cdot10^{-2}$ | $-6.1\cdot10^{-4}$ |
| S3 (double) | 10h | 87º | 75-80 | 148 | 3.5 | 3114 – 3237 | 525 – 540 | 0.46 – 0.45 | $1.2\cdot10^{-3}$ / $1.3\cdot10^{-3}$ | $-1.1\cdot10^{-2}$ / $-1.3\cdot10^{-2}$ | $-2.9\cdot10^{-4}$ |
| | | | | | | | | 0.58 – 0.57 | $1.3\cdot10^{-3}$ / $1.4\cdot10^{-3}$ | | |

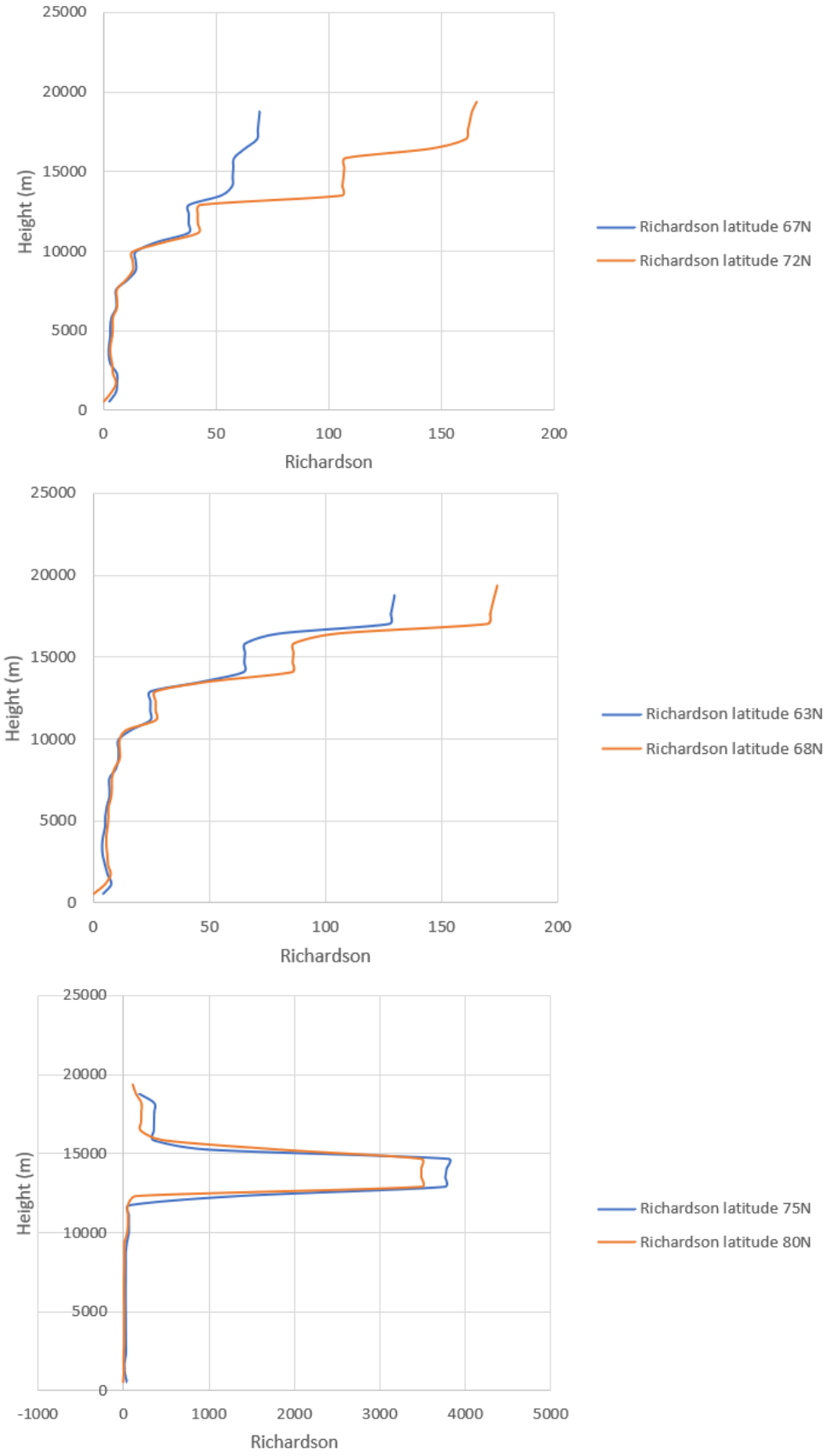


Figure 38. Richardson number as a function of altitude for S1 (top), S2 (middle) and S3 (bottom) [MCD].

With respect of the chosen height for S1 a particular consideration was made. Using MCD the water ice mixing ratio was evaluated in the height interval to help the selection of Z. As it can be seen in Figure 39 the most probable altitude for the water ice clouds to form in the spiral is in the range 0-10 km, which combined with the dU/dz gave a height of 6 km (Table 22).

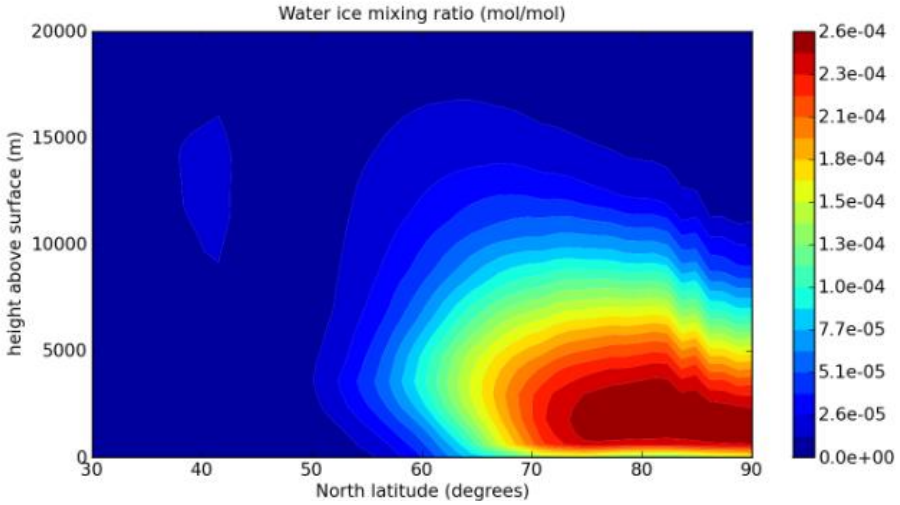


Figure 39. Water ice mixing ratio 0-20 km for the conditions of S1 (May 26$^{th}$ Ls=30$^{o}$, 15h) [MCD].

Based on the results presented in Table 22 all the regions studied verify the Rossby's number condition (Ro<1) and as it can be seen in Figure 38 only in one small interval (12.5-16 km) of S3's region the atmosphere shows a very high Richardson number, above the values expected for baroclinic instabilities to occur. Regarding the $L_D$, all the values obtained verify the condition that the measured length of the spirals, which would work as the horizontal scale ($L_x$ could also be used in this comparison), is far bigger than the $L_D$.

The last point in the theoretical analysis is the comparison of the measured speed of the spirals and the wind's speed values predicted by MCD.

- A speed of 16 ms$^{-1}$ was measured for S1. The MCD model predicts that horizontal speed (in the same direction of the spiral's movement) for the location (latitude and longitude), date and local time of this spiral's development for the altitude range 0-1 km. This is too close to the surface for this kind of feature.
- S2 moved with a speed of 42 ms$^{-1}$. This horizontal speed is predicted by MCD for the spiral's location and local time at the altitude range 8-9 km, which is suitable for this kind of structure.
- The third spiral (S3) moved with a speed of 41 ms$^{-1}$. MCD predicts that horizontal speed for S3's location and local time at an altitude range 5-6 km. This altitude is also suitable for this kind of feature.

This comparison was made with the intention of stablishing a possible height for the spirals but as they are very isolated events it is difficult to assess this aspect from MCD, because this database provides a general overview of the Martian atmosphere.

# 6. CONCLUSSIONS

Using images of VMC and HRSC during the Martian northern spring season (Ls=0º-90º) more than 50 different dynamical structures were identified, with the ADS and the water ice clouds as the most common features. The most interesting are the TDS and the spirals and both were studied deeply.

Unfortunately, one time period of high interest that could not be studied was the aphelion (Ls=71º) because there were no images available from VMC or HRSC (Figure 14, bottom). In the aphelion the isolation of the northern polar cap reaches its minimum at it would have been of high interest to study the formations that develop under this minimum. Figure 14 (bottom) also shows that the temporal distribution (with Ls) of the different features is quite homogeneous, for example, there is a clear tendency in the water ice features as they move to the north with the course of the spring.

Those water ice structures (clouds and hazes) develop near the edge of the polar cap, therefore as the polar cap retreats, they move north. There is a zone (210ºE - 300ºE) with a bigger concentration of them and most of these features are thin clouds with a length of ~ 850 km and a width of ~ 160 km. Whereas, the bigger clouds cover an area of $3.3 \cdot 10^5$ km$^2$ and the hazes an area of $4.7 \cdot 10^5$ km$^2$.

With respect of the TDS, four of them were spotted during the observation period and all of them were observed near Ls=30º, so this period of time can be considered as the most active of the spring season of MY 35. They were all spotted over Acidalia and Amazonis Planitia (150ºE - 210ºE and 40ºN - 75ºN) and their area classifies them as local storms. It has been noted that the size of the storm has an influence on the size of the cells, however the l/w ratio of the cells of each storm can be compared and for the cases where it was analysed the most common ratio was ~ 2.5. Only the speed of two TDS was measured resulting in a mean speed of ~ 32 ms$^{-1}$.

The other dust features studied were the ADS and the so-called dust structures. The ADS appeared during the whole spring season in almost all longitudes with a bigger concentration of them in 300ºE - 350ºE and 50ºN - 70ºN. Their mean size was ~ 1140 km long and ~ 115 km wide. Regarding the dust structures, almost all of them are in the 320ºE - 360ºE and show a mean area of $2.9 \cdot 10^5$ km$^2$.

The other feature that was studied thoroughly was the spirals. Three of them were spotted with one of them composed by water ice and the other ones composed mostly by dust. Two of the appeared in Ls=30º, while the double spiral occurred in Ls=87º. These spirals show a mean length of ~ 1300 km and a mean speed of ~ 33 ms$^{-1}$. The theoretical analysis performed, using the MCD, has clarified that the Martian atmosphere presents the conditions considered as suitable for the features to develop.

To sum up, this project has fulfilled the initial objectives of studying the different dynamical formations that develop in the north polar region during its spring season, besides through the MCD model the atmospheric conditions for the different instabilities to develop have been studied. The results of this Master thesis frame properly in the research developed by the GCP of the EHU/UPV and they will be presented at two scientific international meetings, one in the Europlanet Science Congress [25] and the other one in the Fall meeting of the American Geophysical Union [26].

# 7. REFERENCES

[1] Chicarro, A., Martin, P. & Trautner, R. (2004). The Mars Express mission: An overview. European Space Agency, (Special Publication) ESA SP. 1240. 3-13.

[2] R. Orosei et al. (2018). Radar Evidence of Subglacial Liquid Water on Mars. Science 361 (6401), 490-493.

[3] Ormston, T., Denis, M., Scuka, D., & Griebel, H. (2011). An ordinary camera in an extraordinary location: Outreach with the Mars Webcam. Acta Astronautica, 69, 703-713.

[4] Jaumann, R., Neukum, G., Behnke, T., Duxbury, T. C., Eichentopf, K., Flohrer, et al. (2007). The high-resolution stereo camera (HRSC) experiment on Mars Express: Instrument aspects and experiment conduct from interplanetary cruise through the nominal mission. Planetary and Space Science, 55, 928-952.

[5] Gwinner, K., Jaumann, R., Hauber, E., Hoffmann, H., et al. (2016). The High-Resolution Stereo Camera (HRSC) of Mars Express and its Approach to Science Analysis and Mapping for Mars and its Satellites. Planetary and Space Science, 126, 93-138.

[6] Heavens N. G. (2017). Textured Dust Storm Activity in Northeast Amazonis–Southwest Arcadia, Mars: Phenomenology and Dynamical Interpretation, J. Atmos. Sci., 74, 1011-1037.

[7] Guzewich S. D., Toigo A. D., Kulowski L., Wang H. (2018). Mars Orbiter Camera climatology of textured dust storms, Icarus, 258, 1-13.

[8] Hernández-Bernal, J., Sánchez-Lavega, A., del Río-Gaztelurrutia, T., Hueso, R., Cardesín-Moinelo, A., Ravanis, E. M., Tivov, D., & Wood, S. (2019). The 2018 Martian Global Dust Storm over the South Polar Region studied with MEx/VMC. Geophysical Research Letters, 46(17-18), 10330-10337.

[9] Christensen, P.R., Engle, E., Anwar, S., Dickenshied, S., Noss, D., Gorelick, N., Weiss-Malik, M., Piacentine, N., *JMARS – A Planetary GIS*, http://adsabs.harvard.edu/

[10] F. Forget et al. (1999). Improved general circulation models of the Martian atmosphere from the surface to above 80 km. Journal of Geophysical Research 104, 24155–24176.

[11] E. Millour et al. (2018). The Mars Climate Database (Version 5.3). Scientific Workshop: "From Mars Express to ExoMars".

[12] Sánchez-Lavega, A., Chen, H., Ordóñez-Etxeberria, I., Hueso, R., Río-Gaztelurrutia, T., Garro, A., Cardesin-Moinelo, A., Titov, D., Wood, S. (2017). Limb clouds and dust on Mars from images obtained by the Visual Monitoring Camera (VMC) onboard Mars Express. Icarus. 299.

[13] Kahre, M. A., J. R. Murphy, and R. M. Haberle (2006), Modeling the Martian dust cycle and surface dust reservoirs with the NASA Ames general circulation model, J. Geophys. Res., 111.

[14] Cantor, B. A., James, P. B., Caplinger, M., and Wolff, M. J. (2001). Martian dust storms: 1999 Mars Orbiter Camera observations, J. Geophys. Res., 106 (E10), 23653– 23687.

[15] Ordonez-Etxeberria, I., Hueso, R., Sánchez-Lavega, A., Vicente-Retortillo, A., (2020). Characterization of a local dust storm on Mars with REMS/MSL measurements and MARCI/MRO images, Icarus, Volume 338, 113521, ISSN 0019-1035.

[16] Sánchez-Lavega, A., Perez-Hoyos, S., Hueso, R. (2004). Clouds in planetary atmospheres: A useful application of the Clausius–Clapeyron equation. American Journal of Physics - AMER J PHYS.

[17] Wang, H. (2007). Dust storms originating in the northern hemisphere during the third mapping year of Mars Global Surveyor, Icarus, Volume 189, Issue 2, 325-343.

[18] Wang, H. (2018). Cross-Equatorial Flushing Dust Storms and Northern Hemisphere Transient Eddies: An Analysis for Mars Year 24. Journal of Geophysical Research: Planets. 123.

[19] Martin, L. J., and Zurek, R. W. (1993). An analysis of the history of dust activity on Mars, J. Geophys. Res., 98 (E2), 3221– 3246.

[20] Cantor, B. A., James, P. B., Caplinger, M., and Wolff, M. J. (2001). Martian dust storms: 1999 Mars Orbiter Camera observations, J. Geophys. Res., 106 (E10), 23653– 23687.

[21] Cantor, B. A., (2007). MOC observations of the 2001 Mars planet-encircling dust storm, Icarus, Volume 186, Issue 1, 60-96.

[22] Kulowski, L., Wang, H., Toigo, A. D., (2017). The seasonal and spatial distribution of textured dust storms observed by Mars Global Surveyor Mars Orbiter Camera, Advances in Space Research, Volume 59, Issue 2, 715-721.

[23] Sánchez-Lavega, A., Garro, A., del Río-Gaztelurrutia, T., Hueso, R., Ordoñez-Etxeberria, I., Chen Chen, H., et al. (2018). A seasonally recurrent annular cyclone in Mars northern latitudes and observations of a companion vortex. Journal of Geophysical Research: Planets, 123, 3020– 3034.

[24] Sánchez-Lavega, A., (2011). An Introduction to Planetary Atmospheres, Taylor-Francis-CRC, Florida (USA).

[25] Sanchez-Lavega, A., Garcia-Morales, J., Hernandez-Bernal, J., del Rio-Gaztelurrutia, T., Hueso, R., Ravanis, E., Cardesín-Moinelo, A., Titov, D., Wood, S., Tirsch, D., Hauber, E., and Matz, K.-D.: Patterns in textured dust storms in Mars North Pole, Europlanet Science Congress 2020, online, 21 September–9 Oct 2020, EPSC2020-141, 2020

[26] Sánchez-Lavega, A., García-Morales, J., Hernandez-Bernal, J., del Rio-Gaztelurrutia, T., Hueso, R., Ravanis, E., Cardesín-Moinelo, A., Titov, D., Wood, S., Tirsch, D., Hauber, E., Matz, K.-D., Atmospheric spirals in spring time on the edge of the North Pole of Mars, American Geophysical Union, Fall Meeting, 1-17 December 2020.

Other sources of information have been used in this project but as they are not scientific publications a different category has been created for them.

[w1] Wikipedia, List of missions to Mars (2020). https://en.wikipedia.org/...

[w2] ESA, VMC – Mars Webcam account in Twitter. https://twitter.com/esamarswebcam

[w3] ESA, VMC The Mars Webcam gallery in Flickr. https://www.flickr.com/photos/esa...

[w4] ESA, The Seasons on Mars (2019). https://sci.esa.int/s/WePDvmw

[w5] GIMP. https://www.gimp.org/

## ***ACKNOWLEDGEMENTS***

I would like to end this document with a few words dedicated to the people that have made this project possible particularly taking into account the special circumstances that have affected us all.

The first person I must give my appreciation is the director of this project Prof. Agustín Sánchez Lavega, which has always presented a total availability to assist with the different challenges that this project has presented. His expertise and knowledge in the field of planetary sciences have been a key factor in the development of this project.

The second person that has been of great assistance in the implementation of this project is Jorge Hernández Bernal, whose work with the Elkano application has made possible the measurements techniques used in VMC's images. He has also helped to fix the different issues that the application has presented.

I would also like to thank the members of the evaluation's committee the time they have dedicated to read and review this project.